Winter 12-17-2016

Observations and Light Curve Analysis of Transiting Extra-Solar Planets

Clark M. Holcomb
Stephen F Austin State University, cmholcomb1@yahoo.com

Observations and Light Curve Analysis of Transiting Extra-Solar Planets

Observations and Light Curve Analysis of Transiting Extra-Solar Planets

by

Clark M. Holcomb, B.S.

Presented to the Faculty of the Graduate School of

Stephen F. Austin State University

In Partial Fulfillment

of the Requirements

For the Degree of

Master of Science

STEPHEN F. AUSTIN STATE UNIVERSITY

December 2016

Observations and Light Curve Analysis of Transiting Extra-Solar Planets

By

Clark M. Holcomb, B.S.

APPROVED:

_____
Dr. W. D. Bruton, Thesis Director

_____
Dr. N. L. Markworth, Committee Member

_____
Dr. H. D. Downing, Committee Member

_____
Dr. R. B. Friedfeld, Committee Member

_____
Richard Berry, D.M.A
Dean of the Graduate School

ABSTRACT

The purpose of this research was to perform the procedures to study transiting exoplanets in their entirety, from the data collection process to determining physical characteristics and orbital properties. The research was conducted with two telescopes of different sizes (16” and 12”) at multiple sites in order to refine the detection process. Both Maxim DL and Mira Pro x64 software were used to process the resulting images. The PHOEBE program was used to model the data to determine the properties of the exoplanets, which were then compared to the results obtained by other astronomers. The data collection process as well as the modeling successfully yielded results that were in agreement with the comparison values.

ACKNOWLEDGMENTS

I would like to thank the following individuals for their assistance in this research project: Dr. Bruton, my thesis advisor, who spent many nights assisting me with the telescopes and equipment and Mr. Michaels, who spent time with me discussing imaging techniques, assisting with observations, and especially for allowing me to use his observatory and equipment. I would not have been able to complete this research without their help and support.

TABLE OF CONTENTS

LIST OF FIGURES

LIST OF TABLES

CHAPTER ONE

INTRODUCTION

Exoplanets, short for extra solar planets, are planets outside our solar system that orbit other stars besides the Sun. An exoplanet transit occurs when the planet's orbit causes it to pass in front of its host star, from the observer's perspective, and blocks some of the incoming light from the star (Fig. 1-1).

In order to observe and analyze data from an exoplanet transit, a light curve is used. A light curve is a graph of intensity of the star versus time. When the exoplanet transits the star, some of the light from the star is blocked, and there is a dip in the intensity on the light curve. Therefore, by taking many images of a star over a long period of time, and then analyzing the images, it is possible to see the dips in intensity, and thus find exoplanets.

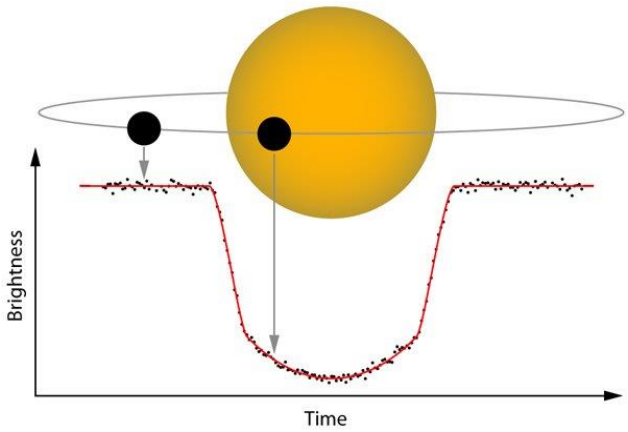

Figure 1-1: Exoplanet Transit
As an object passes in front of the star the brightness of the star will lower as seen in the dip in the graph below the image.

From a transit, astronomers can determine the existence of an exoplanet about the star but can also determine properties of the exoplanet itself, such as its mass, size, density, orbital radius, orbital velocity, orbital period, orbital inclinations, and atmospheric properties.

Objectives

The objectives of this research are:

1. Make photometric observations of several exoplanets and refine the data collection process.
2. Analyze the photometric measurements using photometry software and obtain a light curve for each exoplanet transit observed.
3. Model the exoplanet transits using modeling software called PHOEBE to estimate the mass, radius, semi-major axis, and orbital inclination.
4. Compare the results to the known properties obtained from other observers.

Methods of Measurement

Transit. This method will be used in this paper and is discussed in the above section. As mentioned above, this method can be used not only to detect

the presence of an exoplanet, but also to study and determine physical characteristics about the planet.

The first calculation is the semi-major axis (commonly used as the orbital radius), which can be calculated directly from Kepler's third law of planetary motion.

$$\frac{a^3}{P^2} = \frac{G(M+m)}{4\pi^2} \rightarrow a = \sqrt[3]{GM\left(\frac{P}{2\pi}\right)^2}$$

Where a is the semi-major axis, P is the orbital period, M and m are the masses of the host star and planet respectively, and G is universal gravitational constant. From both the period and semi-major axis it is possible to then calculate the orbital velocity, assuming a circular orbit.

$$v = \frac{2\pi a}{P}$$

The simplest calculation, of which the transit method is particularly useful, is the radius of the exoplanet. This is determined by the amount of light that the planet blocks. When looking at the brightness of a star, the actual quantity being evaluated is the flux, which is the energy radiated per unit time per unit area. Thus, the change in flux as the planet passes in front of the star (the dip in magnitude) is proportional to the fraction of total light being blocked, and thus proportional to the size of the planet compared to the size of the star.

$$\frac{\Delta F}{F} = \left(\frac{r}{R}\right)^2$$

Where ΔF is the observed change in flux during the transit, F is the star flux, while R and r are the radius of the star and planet respectively. This equation assumes the stellar disk has uniform brightness, which is not the case when limb darkening is taken into account, but works well as an estimation (Wilson The Transit Light Curve 2013).

The mass can be found from observing a transit by using Newton's law of universal gravitation.

$$F_g = \frac{GMm}{a^2}$$

Where F_g is the force of gravity between the star and the planet. This can be obtained from radial velocity measurements (discussed later in this chapter). The radial velocity method will provide the minimum possible mass of the planet. The orbital inclination is necessary in order to refine the calculation to determine a more precise value of the mass (Wilson The Transit Light Curve 2013).

$$\text{minimum mass} = m\sin(i)$$

Where i is the orbital inclination. Using the planetary mass and volume (calculated from the planetary radius) it is then possible to calculate the density.

As stated above, the orbital inclination is necessary to determine an exact mass in conjunction with the minimum mass acquired from radial velocity measurements. Determining the inclination usually requires a value called the impact parameter, b. The impact parameter is defined as the sky-projected

distance between the center of the stellar disk and the center of the planetary disk at conjunction (the point in the orbit where the two objects are most closely aligned as viewed from Earth) (Wilson The exoplanet transit method 2016). This in turn requires the time duration of the full eclipse, t_F, and the time duration of the total eclipse, t_T. The diagram below (Fig. 1-2) illustrates the values defined above (Waldmann n.d.).

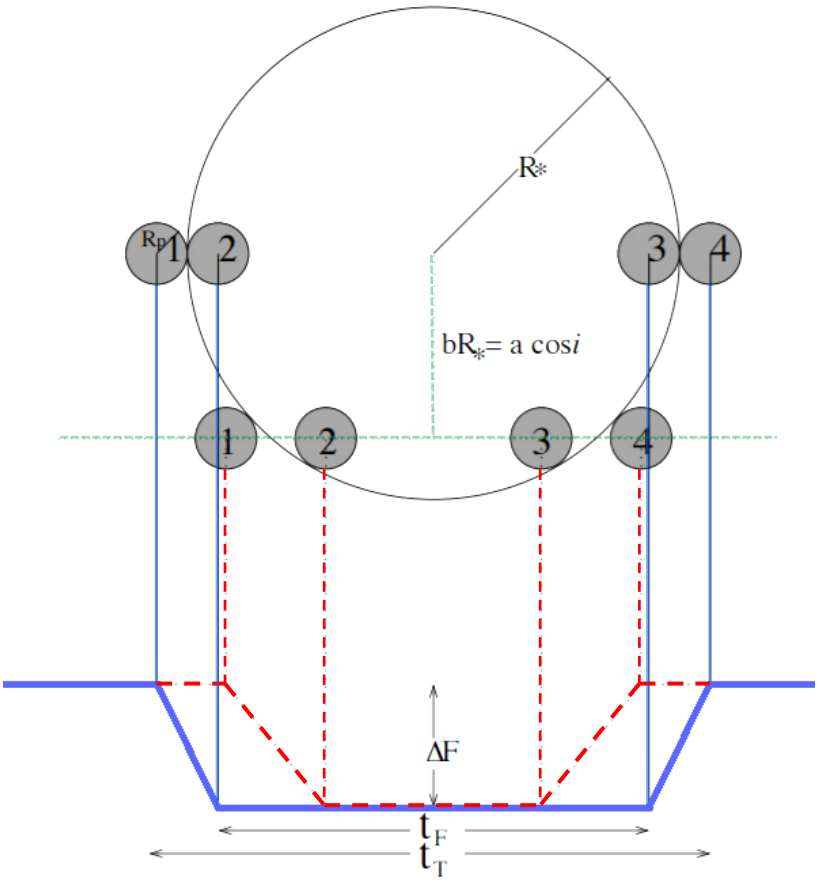

Figure 1-2: Transit Diagram
Diagram detailing the positions of a transiting exoplanet with two different orbital inclinations and the effects on the light curve, with associated labels.

The impact parameter can be calculated using the following equation.

$$b = \left[\frac{\left(1 - \sqrt[2]{\Delta F}\right)^2 - \left(\frac{t_F}{t_T}\right)^2 \left(1 + \sqrt[2]{\Delta F}\right)^2}{1 - \left(\frac{t_F}{t_T}\right)^2}\right]^{\frac{1}{2}}$$

Once the impact parameter has been found, the inclination is gained from the following equation.

$$i = \cos^{-1} b \frac{R}{a}$$

As it will be shown later, it is also possible to approximate the mass and inclination through modeling of the light curves. In that instance, the mass is found as a ratio of the star and planet.

If the planet possesses an atmosphere, then as the planet passes in front of the star, known as the primary transit, some of the star's light will pass through this atmosphere and get absorbed at different wavelengths. This absorption spectrum depends on the specific chemical elements present within the atmosphere. A secondary transit, when the star passes behind the star, will then show the absorption spectrum the star alone. Subtracting spectrum of the secondary transit from the spectrum of the primary transit will produce the true absorption spectrum of the planet. By analyzing the spectrum, it is possible to determine the composition of the atmosphere as well as the temperature (The Planetary Society n.d.)

Radial Velocity. This method measures changes in a star's radial velocity (its relative velocity toward or away from Earth) as the star and planet orbit about their common center of mass. As the star and planet orbit the center of mass, the star will periodically move slightly toward and away from Earth, which will produce a Doppler shift (Fig. 1-3). A Doppler shift is the shift of the emission lines of a star towards the red or blue end of the visible electromagnetic spectrum, which indicates the star is moving with some radial velocity. A redshift indicates a radial velocity away from the observer, while a blueshift indicates a radial velocity towards the observer. These periodic Doppler shifts can be measured to infer the presence of an exoplanet. This method was the first to successfully identify the existence of an exoplanet, 51 Pegasi b, and has since been used to find hundreds more (Mayor & Queloz 1995). In recent years it is used more as a secondary method of verification, as the transit method has become more widespread due to its efficiency and its ability to provide more detailed information about the exoplanet (Mayor & Queloz 1995).

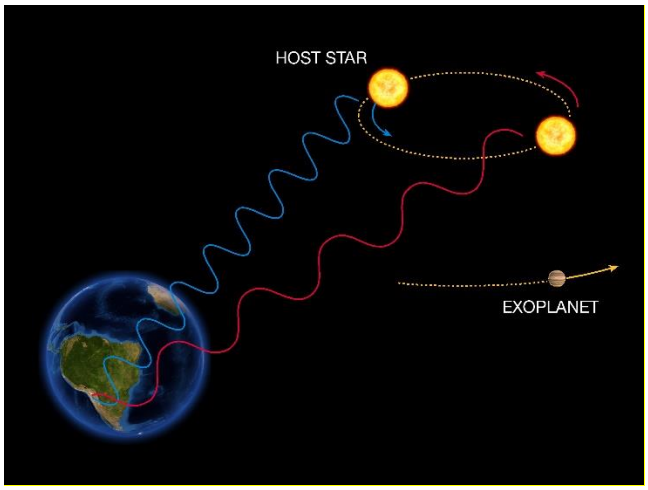

Figure 1-3: Radial Velocity Method
The star appears to wobble in space due to the effect of the planet's gravity. This motion can be detected via the Doppler shift.

Astrometric. Similar to the radial velocity method, this method relies on the small perturbations of the star as it orbits about its common center of mass with the planet. Whereas the radial velocity method depends on the orbital plane being edge-on with Earth, the astrometric method works when the orbital plane is perpendicular to Earth and measures the star's change in position relative to the background stars (Fig.1-4). This method has only been successful in recent years due to the difficulty in making measurements precise enough to obtain useful data. So far only a very small number of exoplanets have been discovered this way (ESO.org n.d.).

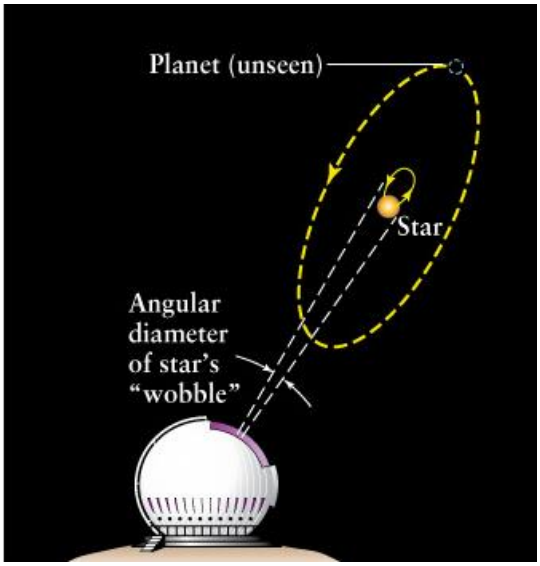

Figure 1-4: Astrometric Method
Similar to the radial velocity method, this technique works when the exoplanet's orbital plane is perpendicular.

Direct Imaging. This method of simply taking an image of the exoplanet directly is particularly difficult due to the parent star being so much larger and brighter than the companion planet. In order to use this method, the light from the star must be blocked or dimmed in order to detect the light from the planet. One technique is to use a device called a coronagraph, built inside the telescope, to block the bright central core of the star. The other technique primarily used is to take infrared radiation images instead of visible light because whereas a star's visible light output can be one billion times greater than that of a Jupiter sized planet, the contrast in the infrared output is reduced to a factor of a few thousands, especially if the planet is still young and contracting, thus producing

heat (The Planetary Society n.d.). Even with these techniques, conditions such as having a large orbital radius or unusually bright planet must be met in order for this method to work. Despite these factors, a handful of exoplanets have been discovered with this method, including Fomalhaut b and Beta Pictoris b (Fig. 1-5), though it is not suitable for large scale surveys searching for exoplanets (Mayor & Queloz 1995).

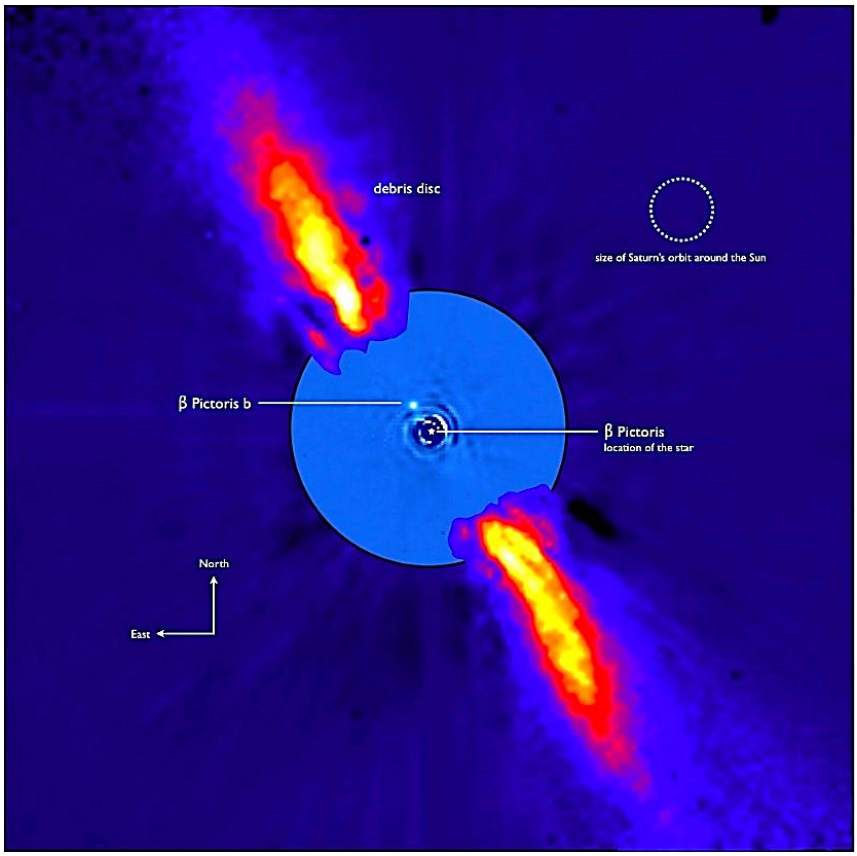

Figure 1-5: Direct Imaging
Image of Beta Pictoris b as seen in the near infrared after the subtraction of the much brighter stellar halo.

Gravitational Microlensing. Predicted by Einstein's General Theory of Relativity, gravitational microlensing occurs as the gravitational pull from a large object bends and amplifies the light from a distant background object, similar to a magnifying glass. This can be used to study stars, black holes, and other distant and difficult to see phenomenon, as long as the foreground object and luminous background object are aligned. If the foreground star is hosting a planet, and that planet is positioned so that it crosses the path of the bending light, then that planet will further bend the light. This causes an additional spike to one side of the image created from the microlensing event, indicating the presence of an exoplanet with a high degree of accuracy as seen in figure 1-6 (The Planetary Society n.d.). This method is unique in that it can find exoplanets at far greater distances than the other methods, however it can only be done once, as these microlensing events are each unique, as well as rare, and do not repeat themselves. Because of this, as well as being unpredictable, only a small number of exoplanets have been discovered this way (Mayor & Queloz 1995).

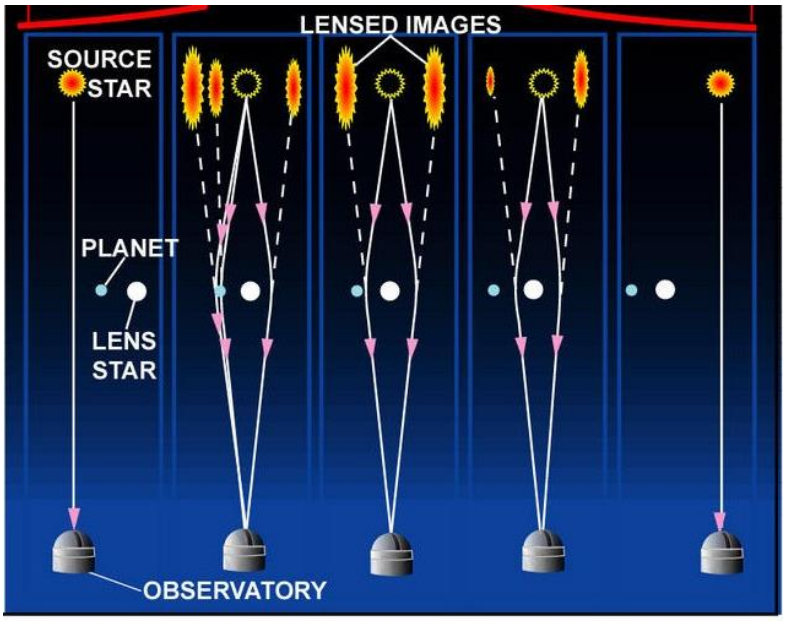

Figure 1-6: Gravitational Microlensing
The microlensing process from right to left.

Literature Review

Exoplanets are designated by the name of their host star, followed by a letter, starting with “b” and continuing in the order of discovery. The host star is considered to be “a”.

WASP-1b is located in the constellation Andromeda, orbiting the star WASP-1, an F7V type star 379pc. This planet was discovered in 2006 via the transit method by SuperWASP, after which it is named. Follow up observations were made with the SOPHIE spectrograph at the Observatoire de Haute-Provence, after which the radial velocity method to confirm it, as well as estimate the mass, radius, and orbital period (Collier Cameron et al. 2006). Since then

approximately 68 papers have been published either about or mentioning WASP-1b (Exoplanet TEAM 2015).

Also discovered via the transit method by SuperWASP in 2008 is WASP-12b orbiting a G0 star 427pc from Earth in the constellation Auriga (Torres et al. 2007). WASP-12b is unique in its proximity to its star, its low density, and the possible possession of a large moon (Chan et al. 2011). There have been approximately 121 publications concerning or referencing WASP-12b (Exoplanet TEAM 2015).

Hat-P-1b was discovered in 2006 by the HATNet project via the transit method orbiting a G0V star 139pc away in the constellation Lacerta. Approximately 78 papers or works have been published either about or mentioning Hat-P-1b (Exoplanet TEAM 2015).

Hat-P-3b was discovered in 2007, also by the HATNet project via the transit method, and later confirmed by Doppler spectrography with the FLWO 1.5m Tillinghast reflector (Burke et al. 2007). This exoplanet is known to have a heavy element rich composition (Starling 2014). Its host star is a K class star of distance 130pc in the constellation Ursa Major. There have been approximately 44 publications concerning or referencing Hat-P-3b (Exoplanet TEAM 2015).

XO-2Nb is 149pc away in the constellation Lynx orbiting the fainter component of the XO-2 binary star system with XO-2N classified as a K0V class star. Discovered in 2007 via the transit method by using the XO telescope in

Hawaii. There have been approximately 70 publications concerning or referencing XO-2Nb (Exoplanet TEAM 2015).

Below is a table listing some of the known properties for each of the above exoplanets.

Planet	WASP-1 b	WASP-12 b	HAT-P-1 b	HAT-P-3 b	XO-2N b
Distance (Parsec)	379	427	139	130	149
Jupiter Masses (M_J)	0.86	1.404	0.525	0.591	0.62
Jupiter Radii (R_J)	1.484	1.736	1.319	0.827	0.973
Semi-Major Axis (AU)	0.0382	0.0229	0.0556	0.0389	0.0369
Orbital Period (days)	2.52	1.09	4.465	2.8997	2.62
Eccentricity	0	0	0.067	0	0.045
Inclination (deg.)	88.65	86	85.634	87.07	88.7
Temperature (K)	-	2525	1322	-	-
Density (g/cm^3)	-	0.337	-	1.06	-

Table 1-1: Known Properties
These are known characteristics for each of the chosen targets.

A CCD (Charged-Coupled Device) imager is used to capture images of what the telescope is observing. CCD imagers work by capturing light from the telescope, after which it is converted into an equivalent charge which is stored in capacitors within the device. The capacitors act as potential wells, storing electrons, where the number of electrons, and thus the electric charge, is proportional to the intensity of the incoming photons. Once the photons are collected, the potential wells are emptied and read one by one, and converted into pixels which make up the final image on the computer screen. The photon collection period is referred to as the exposure time and varies based on what is being imaged, with dimmer objects requiring longer exposures in order to capture more light. Eventually, if the exposure time is long enough, the potential wells can become “full” after which incoming photons will no longer be registered. This is called saturation. Test images are taken at increasing exposure times to look at the saturation of the brightest pixels in the image of the target. The optimum exposure time is chosen such that the pixels are bright enough to generate useful images without presenting the possibility of becoming fully saturated during the observation window.

CCD imagers also possess the ability to bin the pixels in the image. Binning is the process of combining charges from adjacent pixels in order to modify the image quality for various purposes. Default is 1x1 binning where each pixel is its standard size. 2x2 binning then creates pixels that are 2 pixels by 2

pixels essentially creating larger pixels that are squares with an area of 4 standard sized pixels. Binning can be further increased to 3x3 and 4x4. Binning offers faster readout speeds between images as well as improving the signal to noise ratio (SNR) at the cost of reducing image resolution. In general, the binning is decided based on the seeing conditions on the night of observation but can also be based on the download size when appropriate. When observing exoplanet transits, image quality is not the main concern. The goal is not to make a good-looking image but rather to acquire data on the change in magnitude as the transit occurs. Therefore, the binning is chosen such that the Full Width at Half Maximum (FWHM) is 2 to 3 pixels. In other words, the diameter of the target star in the image is 2 to 3 pixels across. It's also important to consider the SNR in the images as higher binning increases SNR, which gives more accurate data.

Additionally, to acquire clear images that can be processed to receive useful data, the raw images must be cleaned up due to a lot of extra "noise" in the exposure process, consisting of such factors as the heat from the equipment itself and particles on the optics of the telescope. Thus, calibration frames are needed, which consist of bias frames, dark frames, and flat frames, that are taken and removed from the images.

A bias frame is created by taking a CCD image with the shutter closed and an exposure time of 0 seconds. The resultant image is that of the electronic

noise from the CCD chip. Generally, multiple bias frames are taken before the observation and are later subtracted from the light frames.

A dark frame is created by taking a CCD image with the shutter closed, thus blocking all outside light. The result is an image of the noise from the equipment itself. As long as the temperature of the CCD chip is the same for the dark frames as it is for the light frames, and the exposure time is also the same, then the dark frames provide an accurate depiction of the noise from the equipment that will be present in the light frames. Generally, multiple dark frames are taken, both before and after the observation, and then subtracted out of the light frames.

A flat frame is created by taking a CCD image of a flat, evenly illuminated surface in front of the telescope. This results in an image of any particles or matter on the optics of the telescope. Additionally, flat frames account for uneven light distribution across the CCD than can arise from variations in sensitivity from pixel to pixel. These are then divided from the light frames.

Additionally, dark frames sometimes called flat darks can be taken for the same exposure time as the flat frames which are then subtracted from just the flats as these are also subject to the noise from the electronics. This further helps with producing good images for analyzing and can take the place of bias frames if necessary.

Justification

Discovering and studying exoplanets is significant for a number of reasons. First and foremost, discovering them helps in understanding just how common they are in the universe as well as understanding the factors that contribute to their formation and their relationship with their parent star. This in turn can increase our understanding of the formation of our own solar system and its origins. Additionally, the exoplanets can be studied to discover new unique properties for their systems, such as unusual orbital dynamics or atmospheric properties which could answer previously unknown questions about the physical laws of the universe. The observations in this research can help to assist in expanding the database for known exoplanets and their orbital periods, transit times, transit durations, and physical properties of the planets themselves. With the ongoing detection of thousands of exoplanet candidates within the last several years, knowing techniques for detecting them can not only be used to discover new ones but can also assist in confirming the already large number of possible candidates.

CHAPTER TWO

DATA COLLECTION

Selection of Targets

A list of exoplanet was obtained from Gregory P. Laughlin (Laughlin 2009). From this list observation targets were selected based on short orbital periods, coordinates visible within a specific time frame, stellar magnitude, and transit depth. The short orbital periods were necessary in order to insure that the transits were observable within a single night from a ground based telescope, thus also requiring coordinates visible within those specific time frames. The stellar magnitudes were required to be bright enough to be visible with the telescopes being used, while transit depths deep enough to be detectable with the telescopes and CCD cameras were also necessary. The final targets chosen and observed were WASP-1b, Hat-P-1b, WASP-12b, XO-2Nb, and Hat-P-3b.

Telescopes and Observatories

The first observatory used to conduct observations was the SFA Observatory. The telescope used was a Meade LX200GPS 16” Schmidt-Cassegrain telescope (Fig. 2-1) with aperture of 406.4mm, focal length of 4064mm, and using an open fork mount as pictured below.

Figure 2-1: 16" Schmidt-Cassegrain Telescope
Located at the SFA Observatory

After the first several observations, the research was conducted at a different site, the Waffelow Creek Observatory just east of Nacogdoches, due to issues with the tracking and positioning of the 16” telescope that made it unsuitable for transit observations. This observatory uses a GSO 12” Ritchey-Chrétien telescope (Fig. 2-2) with aperture of 304mm, focal length of 2444mm, and mounted on a paramount MX as pictured below. The design of the mount requires the telescope to perform a meridian flip due to its inability to move continuously across the entire sky.

Figure 2-2: 12" Ritchey-Chrétien Telescope
Located at the Waffelow Creek Observatory

CCD Cameras

The SFA Observatory has two CCD cameras, both of which were utilized. For the first two observations, the imager was a model SBIG STL-1301E of size 1280 x 1024 pixels at 16µm, image scale 0.81”/pixel, and field of view of 17 x 14 arc minutes. For the rest of the observations conducted at this site, due to being a newer model with a different filter set, the imager was switched to a model SBIG ST10 of size 2184 x 1472 pixels at 6.8µm, image scale 0.34”/pixel, and field of view of 12.5 x 8.5 arc minutes. Both cameras are shown below in figure 2-3.

The Waffelow Creek Observatory utilizes a model SBIG STXL imager of size 3072 x 2046 pixels at 9μm, image scale 0.76”/pixel, and field of view of 39 x 25 arc minutes.

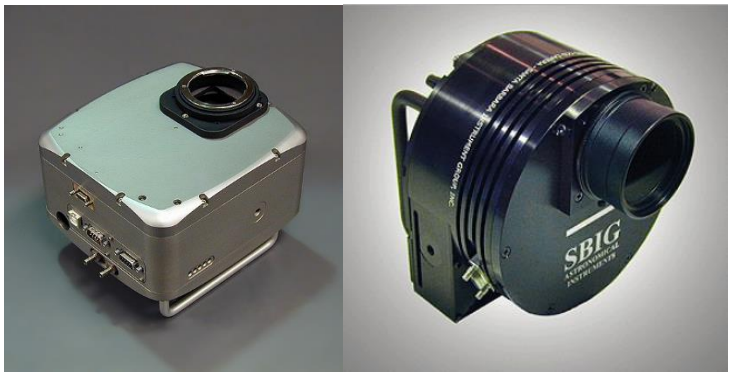

Figure 2-3: CCD Cameras
Left: 1301E, Right: ST10

Flat Field Screen

In order to take necessary calibration images (see procedure section), an Alnitak Flat-Man (Fig. 2-4) was used along with the accompanying software that controls it. It is a flat, wall mounted source of illumination that is specifically designed with the purpose of easily aquiring flat fields. The brightness can be adjusted as necessary to aquire these images under various conditions. Both the SFA Observatory and the Waffelow Creek Observatory utilize this device.

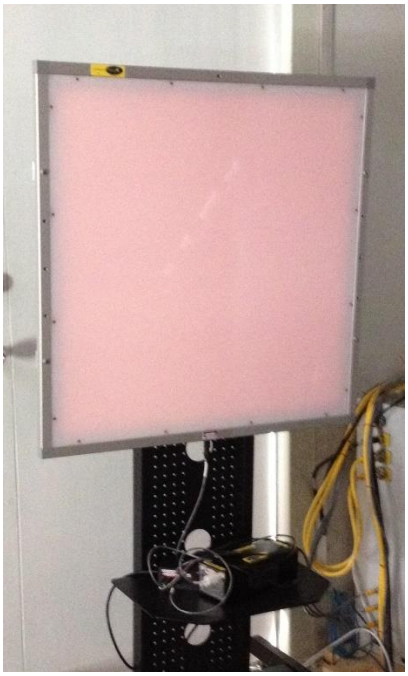

Figure 2-4: Flat-Man XL
Utilized for the creation of flat frames

Data Collection Software

TheSky X is planetarium software that interfaces with the telescope. It allows the user to align the telescope on known stars as well as allows the user to locate target objects. The user can simply click on a target object and slew the telescope to any celestial object in the database. TheSky X was also used to focus the telescope.

Maxim DL is a program that can be used to acquire and process astronomical images. Here the images undergo the data reduction process and

can then be analyzed and plotted as a light curve in order to see any dips that could indicate the presence of an exoplanet.

ACP (Astronomer's Control Panel) is an observatory control software that controls the telescope, CCD camera, and roll-off roof. It controls all these aspects through scripted instructions written by the observer (Fig. 2-6). It also has connections to weather sensors for automatic shutdown in the event of bad weather. ACP interfaces with two other software applications called TheSky X and Maxim DL. ACP was only used at the Waffelow Creek Observatory.

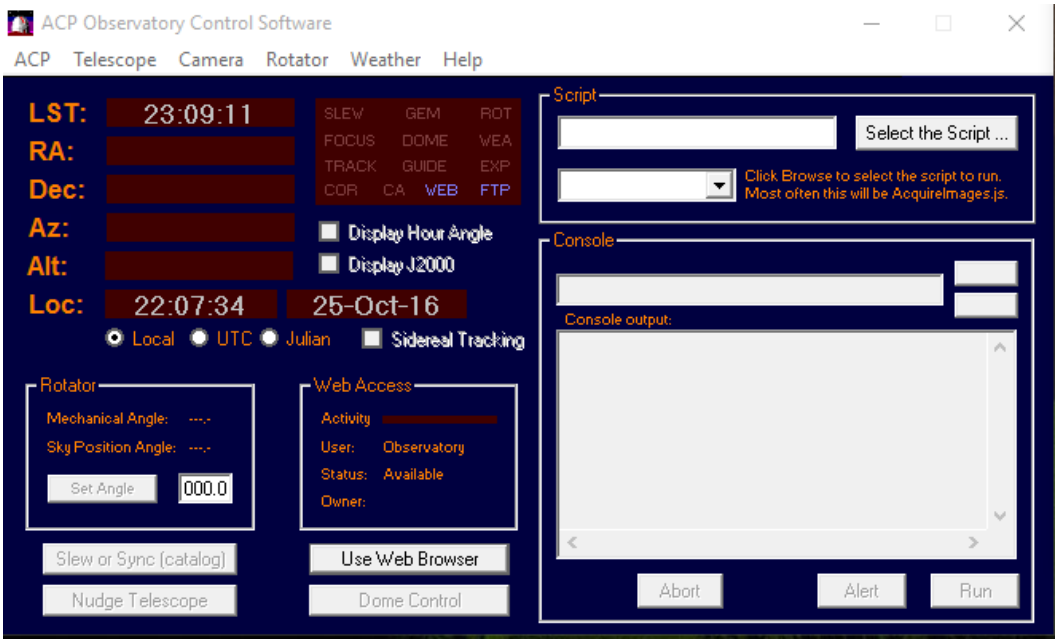

Figure 2-5: ACP Interface

WASP-1 - Notepad

File Edit Format View Help

```
; -----------------------------------------
; This plan was generated by ACP Planner 4.2.6
; -----------------------------------------
;
; For:           Ed
; Location:      Waffelow Creek Observatory
; Coords:        Lat = 31° 41' 55" Lon = 94° 31' 25"
; Targets:       1
; Autofocus at start of run.
;
; -----------------------------------------
;
;
;
;
;
;
;
;
#autofocus
;
#nopreview
#subframe 0.78
;
; === Target GCVS WASP-1 ===
;
;
#count 3000
#filter sR
#interval 20
#binning 1
WASP-1  00:20:40.07     +31:59:24.0
;
;
;
#QUITAT 08:00  ;UTC (03:00am local)
;
;
#CHAINSCRIPT ShutDownObs.js     ; Home and park scope, close roof, warm CCD, power off scope and camera
;
; -----------
; END OF PLAN
; -----------
```

Figure 2-6: ACP Script

An example script (for WASP-1) that tells ACP what actions to perform.

Data Collection Process

First, it is necessary to acquire data by observing an exoplanet transit. Using the NASA Exoplanet Archive (Exoplanet Archive n.d.) and the Exoplanet Transit Database (Exoplanet Transit Database n.d.), the predicted transit dates and times for the chosen targets were acquired and the first observation was made on the first given date which had clear enough skies to observe. The observations were performed at the SFA Observatory. On the first night, September 25, 2015, the equipment necessary to create flat-fields was unavailable, so flat-fields were taken at a later date.

Once the weather was confirmed to be clear, the roof of the 16" telescope housing was opened. The CCD camera was powered on along with the telescope, and given time for the chip to cool down. The target star, WASP-1, was then found with the telescope by utilizing The Sky X as well as existing images of the star field around WASP-1. The telescope is connected to The Sky X where it can then be controlled, after which the right ascension and declination coordinates for the star can be entered in so the telescope will slew to those coordinates in the sky. Once there, the field of view is compared to the existing star field image for the target star to ensure that the telescope is aimed at the correct spot. If not, it must be slowly moved around the area in small increments, until the correct star field is within the telescope's field of view. From here, some test images are taken of the star in order to determine the optimal exposure time

for the imaging process. For the observation of WASP-1b, an exposure of 30 seconds was used along with a luminance filter in order to capture light in the visible spectrum, and binning of 2x2 to decrease the download time of the images between exposures without interfering with image quality. The predicted start time of the transit was 4:18 UT (11:18 local time), so the beginning of the observation was set to at least 1 hour before that. The same is true for all observations. Once the observation began, dark-frames were taken every hour throughout the duration. At the end of the transit observation a total of 516 exposures had been taken. The images were saved to a flash drive to be processed later.

The second target to be observed was the star HAT-P-1 on November 19, 2015. Several issues were encountered during this observation. There were difficulties in properly aligning the telescope as the finder scope on the telescope was damaged and could not be used to help find the targets used for alignment, nor could it be used to assist in finding the target star after alignment. Alignment and finding the target had to be done solely with the CCD camera mounted on the eyepiece. Thus, imaging did not begin until after the estimated ingress time for the transit had passed. The exposure time used was set at 15 seconds using a luminance filter and binning of 2x2. In addition, a delay of 5 seconds was set between each exposure to reduce the total number of images taken so as to reduce the amount of space required to save all of them. Dark frames were once

again to be taken every hour, and 20 flat fields were taken at the beginning of the observation run. It was discovered some time later that there was an auto-dark subtraction setting active on the CCD camera that was performing dark subtractions on the images before displaying them. This affected the exposure time that was chosen for the images as well as producing data that had already been processed to a small but unknown degree. Once discovered and deactivated, the exposure time was reexamined and determined to be only 3 seconds, which led to the delay being increased to 30 seconds. Finally, the observation was ended prematurely as a result of the target star falling below the top edge of the wall of the building that houses the telescope. Over all, approximately half of the predicted transit was observed.

In January 2016, new targets were selected to be observed in the spring semester, with three being observed. The first target to be observed was the star WASP-12 on February 12, 2016. The CCD imager previously used was switched to a different, newer CCD imager that had a different filter set. It was determined that the optimum exposure time for this star is 10 seconds with a binning of 2x2. The filter was changed at this point from luminance to clear, which would let in all wavelengths rather than just visible in an attempt to collect better data. The procedure for taking dark frames was changed to now take 10 dark frames at the beginning and 10 more at the end to eliminate interruptions during the primary image taking process. This was also the first use of the new

flat frame imaging process utilizing the new Flat-Man device and accompanying Alnitak software. The intensity (or brightness) of the flat field was set at 150 and the exposure was set at 0.05 seconds, for 10 flat frames taken at the start. In addition, 10 dark frames were taken with an exposure time of 0.05 seconds which will be subtracted from the flat frames during processing. The purpose of this is to take the place of bias frames. At the end, a total of 1027 exposures had been taken.

For the next target star, XO-2N, the exposure time, binning, dark frames, flat frames, and filter were identical to those previously used for WASP-12. This transit was observed on February 16, 2016. A total of 915 exposures were taken.

The final target of the spring semester was HAT-P-3 observed on May 6, 2016. The exposure time was set to 20 seconds, binning of 2x2, clear filter, with 20 dark frames at the beginning and 20 dark frames at the end. In order to improve the flat frames, it was determined that the intensity should be decreased so as to take longer exposures. Therefore, the intensity was set to 40 and the 20 exposures were 5 seconds in length with the addition of 20 flat-dark frames.

In the Fall of 2016, the same targets were chosen as in the Fall of 2015 to once again to be observed. Due to issues with the 16 inch telescope, at least one being the poor tracking which affected the results, the observations were performed at the Waffelow Creek Observatory, owned by Edward Michaels.

The first target observed during the semester was HAT-P-1 on October 1, 2016. The first step was to create the calibration frames. The bias frames were created first, totalling 30. Then 20 dark frames of 20 second exposure, with the intention of scaling the images to match the exposure length of the light frames using software during the processing stage. Finally, 20 flat frames were taken with a field brightness of 40 and exposure time of 5.5 seconds. From here the telescope was connected to the Sky X and slewed to the target star where an exposure time of 10 seconds was determined to be the optimum exposure. The visual filter chosen due to the brightness of the target star making the dip easily visible, while 1x1 binning was chosen for the purpose of having a high enough image resolution to separate the target star from its visual binary companion in addition to having good seeing on this night. In order to reduce the file size for the images without modifying the above perameters, a subframe was used to cut off the edges of the images and leave only the target star and several comparison stars chosen for processing within the image. At this point, software called ACP was used to perform the observation. This software allows a script to be written telling the telescope what actions are to be performed after which ACP will perform all the actions necessary for the observation. ACP will align the telescope right on the target, focus the image, begin taking images with the correct settings at the appointed time, and, at the appointed end time, will shut down and home all the equipment. No meridian flip was necessary due to the

observation beginning after the star had already crossed the meridian on this night.

The next target was WASP-1 observed on October 2, 2016. The same procedure for the calibration frames was used with the exception of taking 60 second exposures for the dark frames since the exposure length of the light frames would need to be longer due to the dimmer target star. The dimness of this star required that some of the higher frequency light be filtered out to make the dip in the light curve more easily visible. As such, a Sloan Red filter was used with 20 second exposures while still utilizing the same 1x1 binning and subframe as the previous observation. Once again, the observation was made using the ACP software once a script with the proper parameters was written.

HAT-P-1 was observed once again on October 10, 2016, in an attempt to acquire a smoother light curve for modeling. The parameters were adjusted from last time to account for differences in the observing conditions. The seeing on this night was good, so 1x1 binning was used once again. However, due to the presence of a first quarter phase moon, the filter was changed to an sR in order to reduce the higher frequency light in the sky from the moon. This also led to an increased exposure time of 15 seconds. The parameters for the three calibration frames and the procedure for ACP remained the same.

CHAPTER THREE

DATA ANALYSIS

Data Analysis Software

As previously discussed, Maxim DL can be used to process astronomical images and create light curves in addition to obtaining the images.

Mira Pro 64x is another program that, while unable to obtain images, is used to process astronomical images before analyzing them and outputting the data necessary to create a light curve. While performing most of the same processing procedures as Maxim, Mira is more stream-lined and thus quicker in those regards.

PHOEBE (PHysics Of Eclipsing BinariEs) is a program based on the Wilson-Devinney code for modeling eclipsing binary stars based on photometric and spectroscopic data. Although originally for eclipsing binary stars, it can be used to model transiting exoplanets in case by case analyses. During this research, the PHOEBE 0.31a code was used to perform the modeling.

Data Analysis Process

Before generating light curves from the images, they must first undergo data reduction to reduce the noise within the images. This can be accomplished by both Maxim DL and Mira Pro x64. For the observations performed at the SFA

Observatory, data reduction and creation of light curves was done using Maxim DL due to convenience and ease of access. The data reduction process will be detailed in full for both programs starting with Maxim DL.

Maxim DL. First, each of the calibration frame types need to be combined into a single master dark frame and a single master flat frame. Open all the dark frames in Maxim DL. Go to process>combine, and in the window, add all the dark frames (Fig. 3-1).

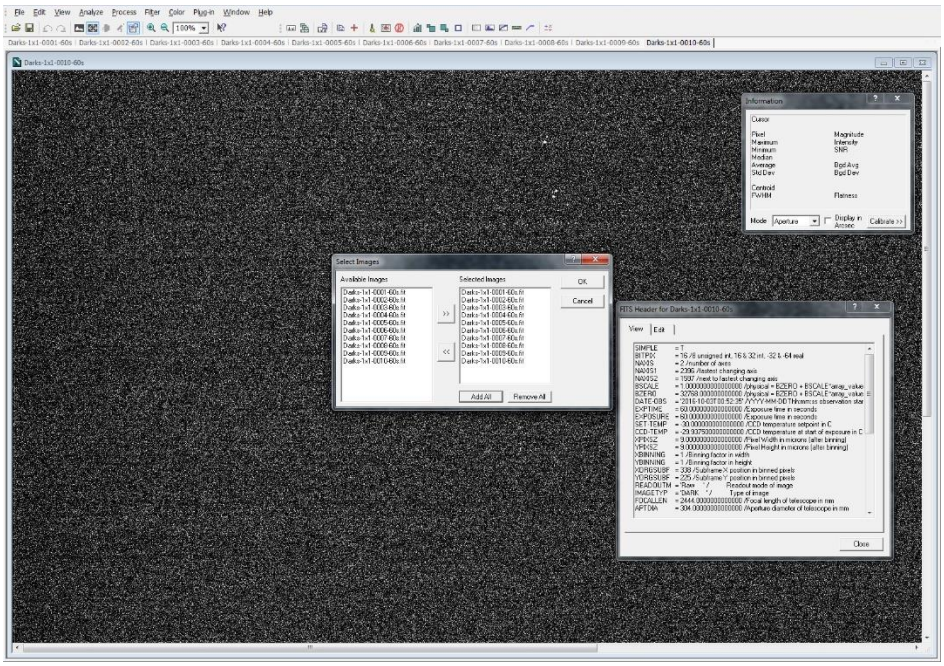

Figure 3-1: Add Calibration Frames

Then in the combine images window, set the output type to median (Fig. 3-2) so as to get rid of any random errors such as cosmic ray bursts that could otherwise appear in the final combination if the output is set to average. Set the

align mode overlay, and from there simply hit overlay all images. The resulting image is the master dark frame.

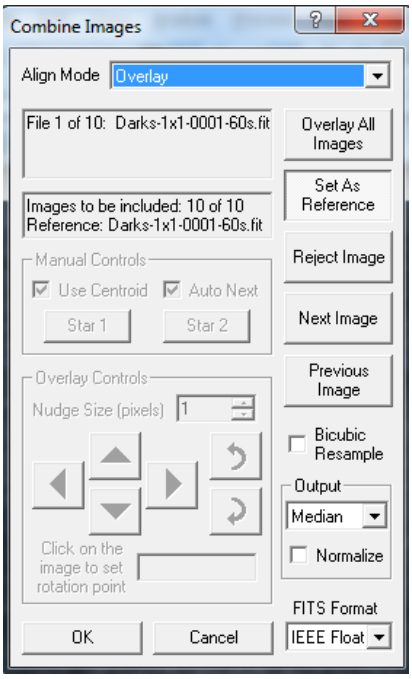

Figure 3-2: Combine Images Window

Follow the same procedure for the flat-dark frames to create a master flat-dark. Then open all the flat frames in Maxim DL and subtract the master flat-dark from all of them. Then the same procedure as before is used to create a master flat frame.

Now open the exposures of the target star in Maxim. Depending on the file size of the individual images, it may not be possible to open them all up at the same time, as was the case with these images. Instead they can be processed in groups of 50 to 100 images at a time. Each group of images needs to be

cleaned up by subtracting the master dark frame and dividing the master flat frame out before creating the light curve. This is accomplished by going to process>set calibration in order to choose the calibration frames that are going to be applied (Fig. 3-3).

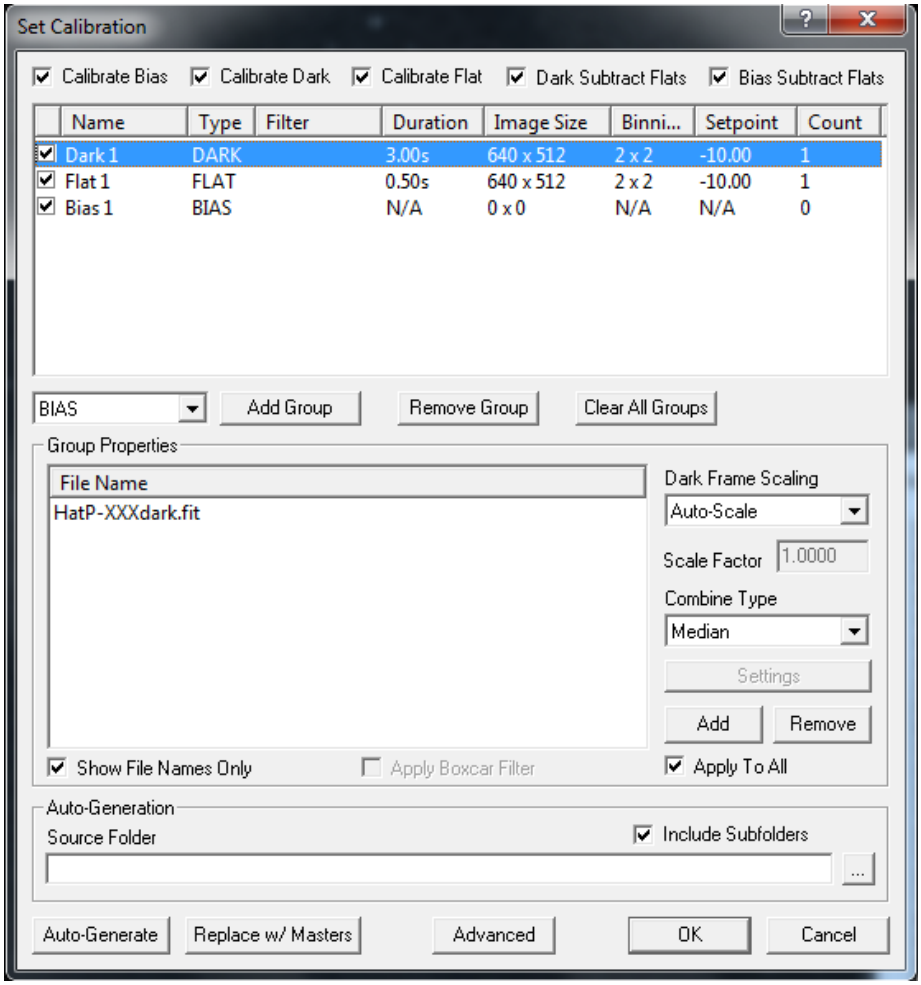

Figure 3-3: Set Calibration Window

For each calibration frame, select the appropriate type of frame from the group dropdown menu, then press Add Group. Select the group and add the

appropriate master calibration frame to said group. Make sure the combine type is set to median for each group before hitting OK. Back on the main screen, go to process>calibrate all, and Maxim DL will automatically apply the calibration frame corrections to all the images currently open. Save these processed images as new images so as not to overwrite the original raw images.

Once the data reduction process is complete, the images can then be analyzed to create a light curve. Go to analyze>photometry, which will bring up an image list and photometry options (Fig. 3-4).

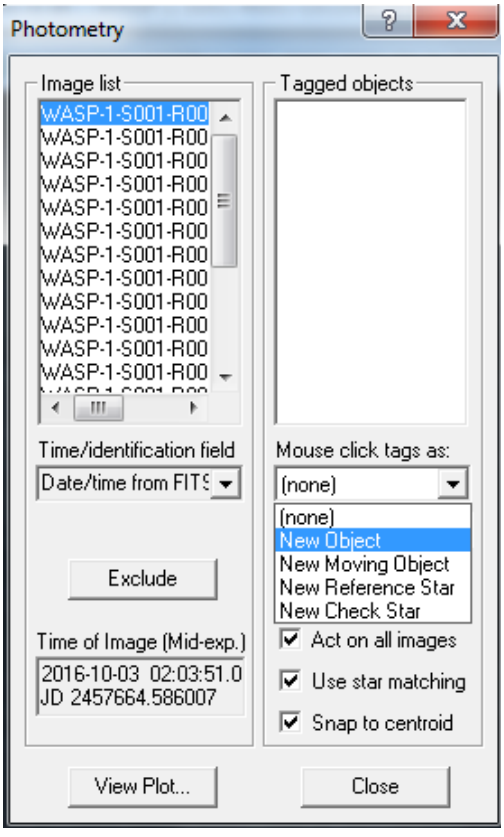

Figure 3-4: Photometry Menu In Maxim DL

Under the Mouse click tags dropdown menu, select new object. Locate the target star in the image and click the mouse in the center of the star. This will place rings around the star in a bullseye pattern as seen in figure 3-5 below.

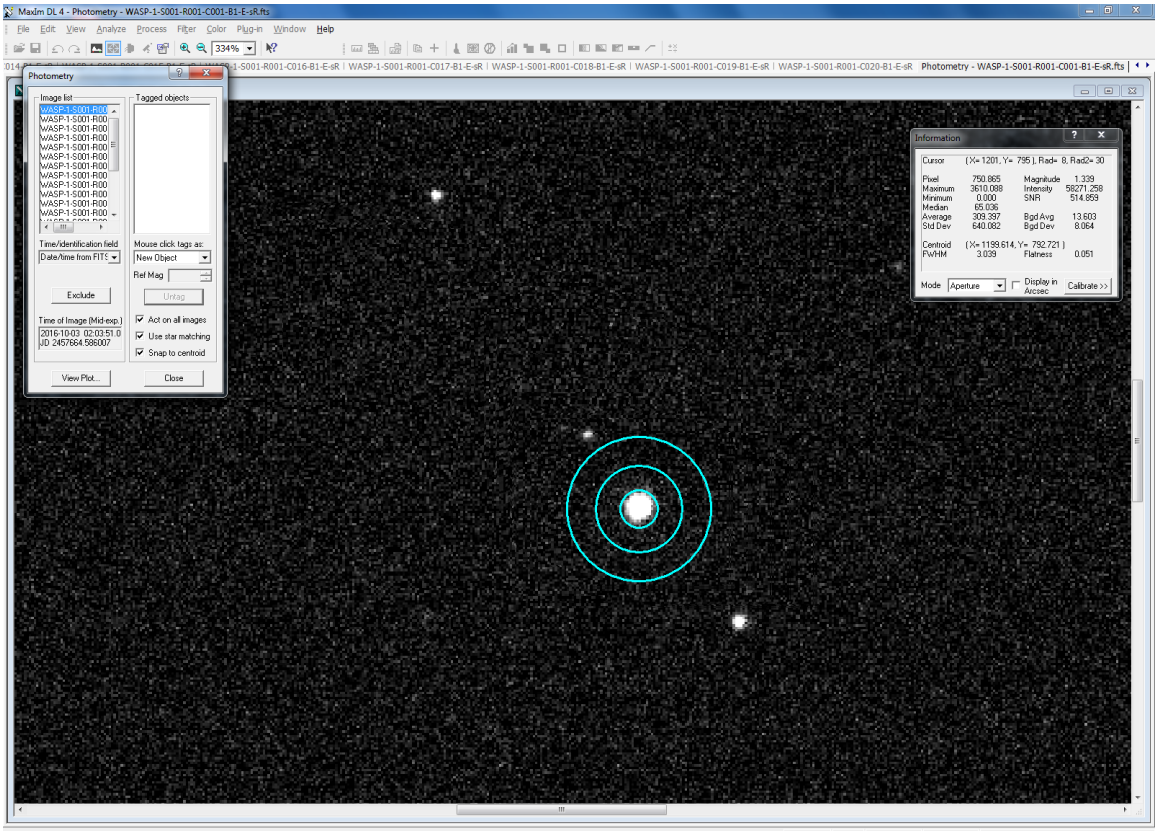

Figure 3-5: Aperture Placement

Each of the three rings has a different purpose in the photometry measurements and can be adjusted in size the gain the most accurate measurements. The inner ring (Aperture) measures the amount of light within it and thus should include all the light from the star while excluding as much of the background as possible. The second ring (Gap Width) serves to isolate the star from the

background, acting as a buffer between the inner and outer ring. Light within this gap width is excluded, and thus any nearby stars should be within this area to be excluded from the light measurements. If there are no nearby objects interfering or bleeding into the target, then the gap width is not always necessary and need not be much larger than the aperture. The final circle (Annulus) measures the average background light to be subtracted from the measurement to determine the brightness of just the target star. The annulus should be as large as possible without including any other stars or objects within it.

Once the target star is selected, Maxim DL will use star matching to place the aperture around the target in the rest of the images. Depending on the seeing conditions and the quality of the images, it may be unable to do this for all the remaining images. If this occurs, Maxim will highlight the images in the image list where they can be excluded from the light curve by pressing the exclude button.

Now select New Reference Stars in the dropdown menu to choose the stars to be compared to the target. A good list of reference stars can be obtained from the American Association of Variable Star Observers (AAVSO). It will provide stars around whichever target is being observed that are of stable and near constant brightness which is ideal when looking for the magnitude dip of an exoplanet transit. For best results, choose more than one reference star to account for any anomalies in brightness that may occur due to atmospheric or

stellar events. Once the reference stars are chosen, click the center of each one to place apertures around them as in figure 3-6.

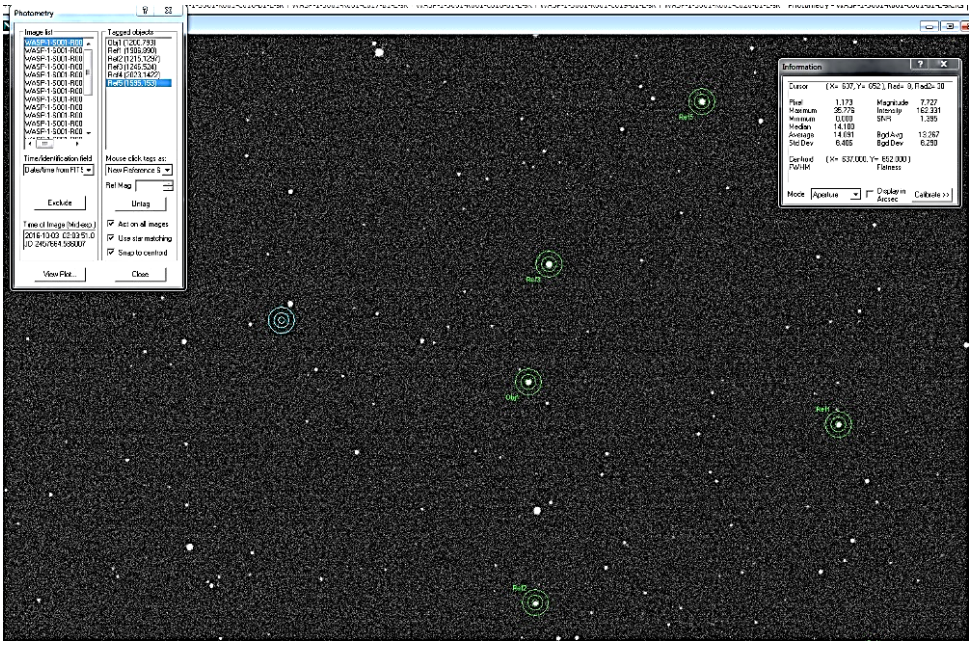

Figure 3-6: Target Star With Reference Stars

The radii of the aperture, gap width, and annulus should be the same for all the reference stars so choose them based on the largest reference star size and proximity of surrounding objects. The radii should also be as close as possible to the radii of the target star so choose reference stars that are close in size and brightness to the target.

Once the target and all the reference stars have been marked, select view plot in the photometry window to view the graph of magnitude versus time for the target and reference stars.

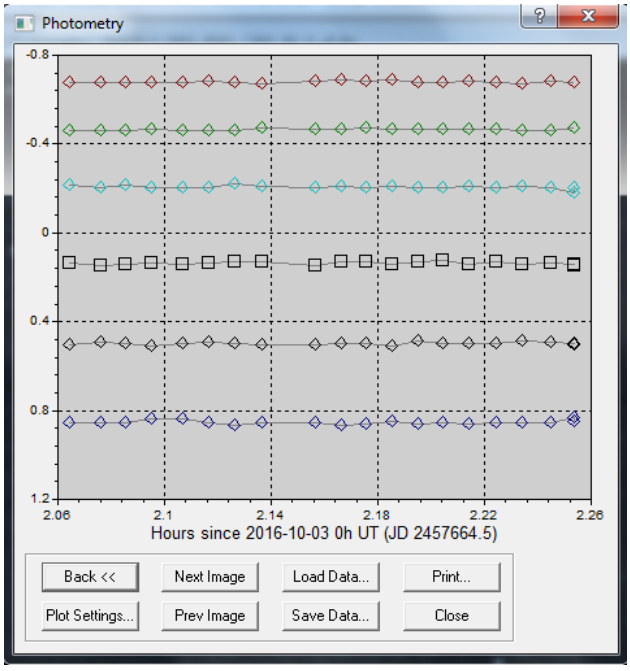

Figure 3-7: Photometry Results From Maxim DL

For good reference stars all the plots should be relatively flat as seen in figure 3-7. Since these are the results for only groups of images rather than all of them, the transit dip will not be visible, and the plot of the target star will appear as flat as that of the reference stars. Save the data and repeat the above procedures for the rest of the images from the observation.

Once all the images have been processed, open all the photometry plots in excel. The plots will simply appear as a list of all the data points. Combine all the different groups in excel and create the magnitude versus time graph for the target star. This will produce the final curve with the visible transit dip.

Mira Pro x64. Once the observations were moved to the Waffelow Creek Observatory, Mira Pro x64 also became available. Image processing from this point was done with Mira Pro x64, because it is quicker and more efficient than Maxim DL. The general procedure for image processing with Mira is the same as Maxim; creating master calibration frames, applying the calibration frames, selecting the target star and the reference stars, measuring the brightness, and creating the final light curve. The specific procedure process is where the two programs differ.

After opening Mira, in the tool bar there is a row of letters X, B, D, and F. These are the calibration menus, where B is for bias frames, D is for dark frames, F is for flat frames, and X is to calibrate the light frames. Start by creating the master bias frame since it does not need to undergo data reduction.

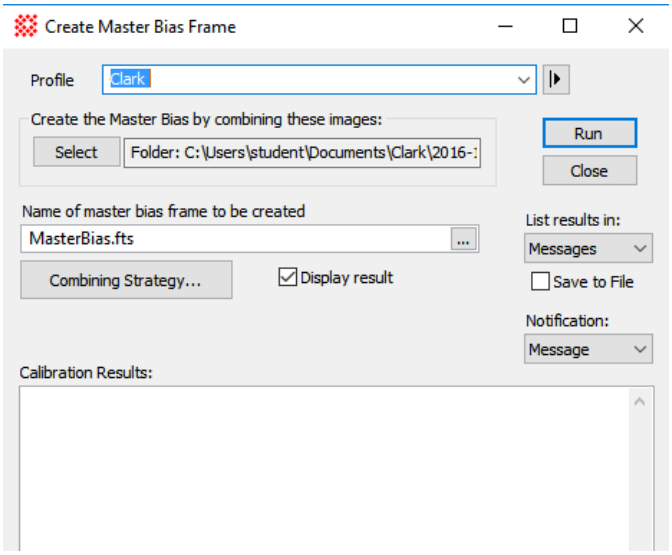

Figure 3-8: Master Bias Window

Below the profile name, click select and choose the file folder that contains the bias images to be combined, then click Run (Fig. 3-8). Mira will automatically pull the correct files from the folder to create the master bias frame without them having to be opened in Mira, while leaving any other files in the designated folder unchanged. Save the new master bias frame in a new folder separate from the raw calibration frames.

The master dark should be created next and will have some extra steps than the creation of the master bias did.

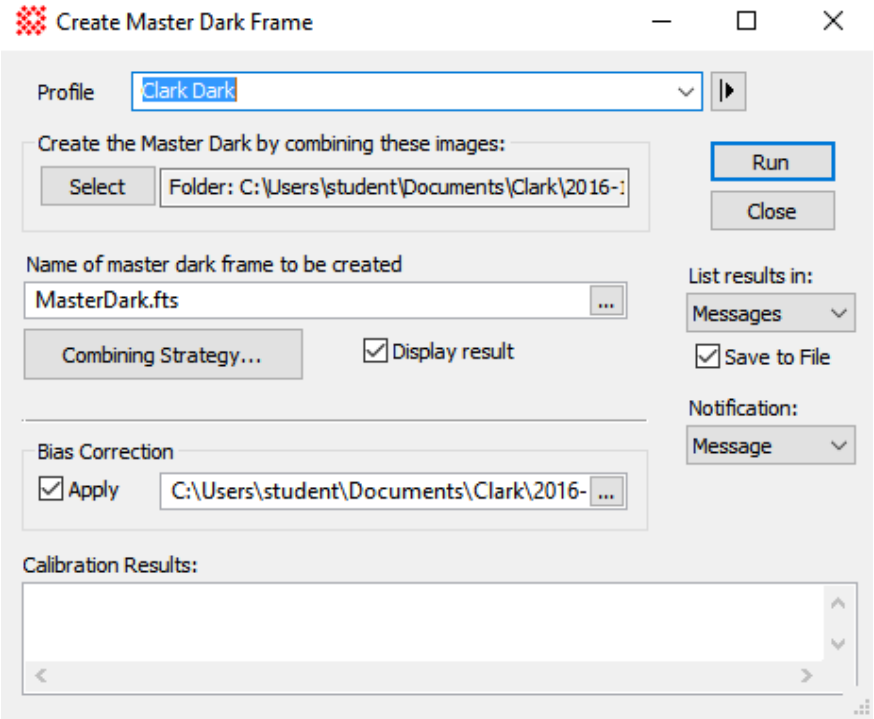

Figure 3-9: Master Dark Window

Similar to the master bias frame, select the folder where the raw dark frames are. Check the box to apply the bias correction and choose the file folder containing the master bias frame (Fig. 3-9). Hit Run, and Mira will automatically subtract the master bias frame from all the dark frames before combining them. Save the new master dark frame in the same file folder as the master bias frame.

Lastly, create the master flat frame.

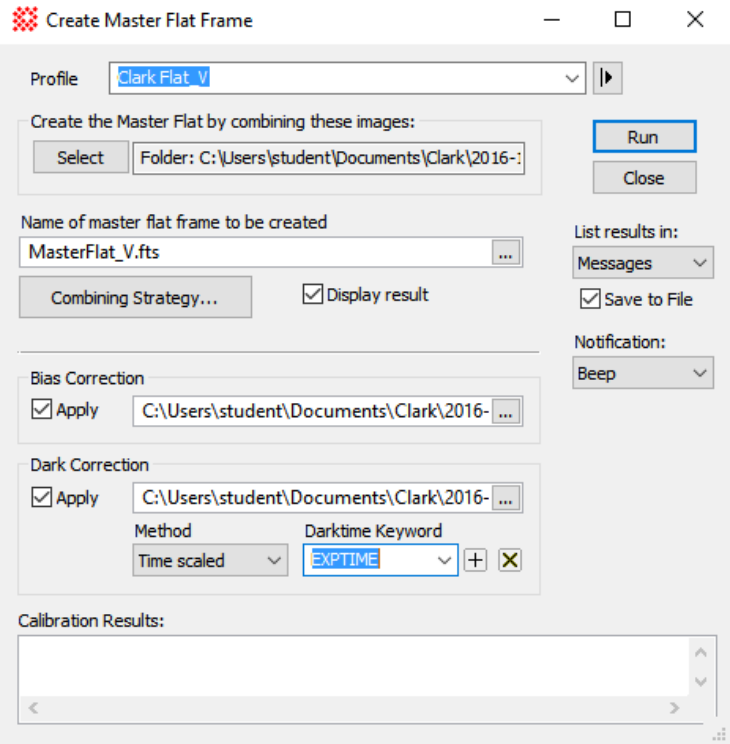

Figure 3-10: Master Flat Window

Once again select the file folder that contains the raw flat frames. Then apply the bias correction and select the file folder containing the master frames (Fig. 3-10). Finally, apply the dark correction and choose the master frame file folder. Also

change the dark correction method to time scaled and make the keyword EXPTIME. Since the exposure time for the dark frames was different than that of the flat frames, this will scale the dark frames down as if their exposure time was matching the flat frames. Then hit Run, and the bias and dark corrections will be applied before creating the master flat frame. Save the master flat in the master calibrations folder.

Now the master frame corrections can be applied to the images.

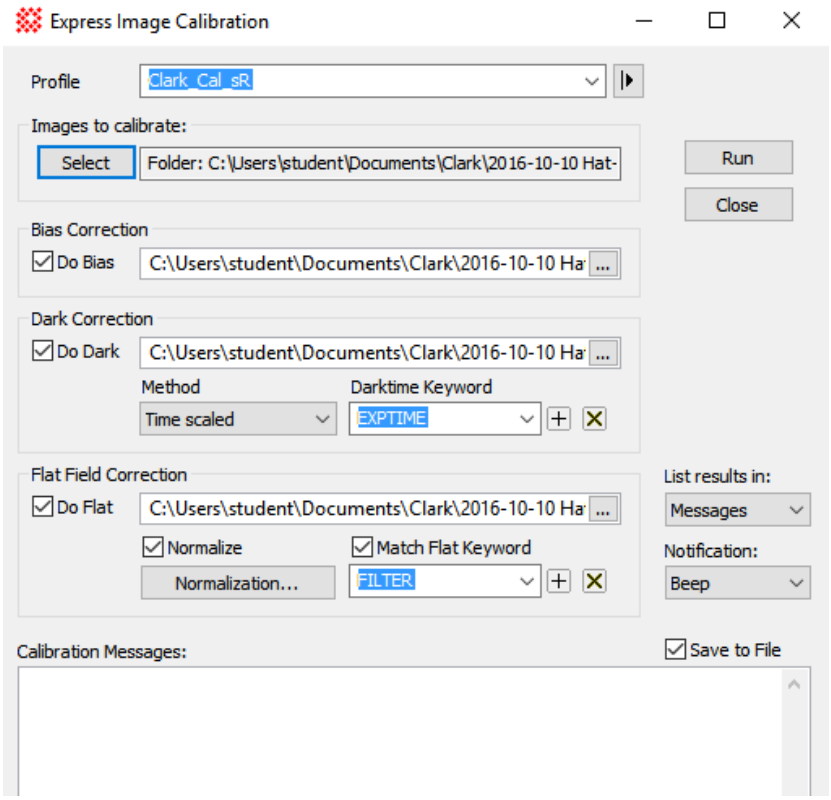

Figure 3-11: Light Frame Calibration

Follow the same procedure as for creating the master calibration frames with the addition of applying the flat field correction (Fig. 3-11). The flat field correction should be normalized and the keyword is FILTER, designating the use of a filter. Make sure there are copies of the original raw images in a separate folder. Then hit run, and the corrections will be applied to all the images.

Now open all the calibrated images in Mira. Open the photometry tab by pressing the button with the bullseye pattern of the photometry apertures located in the tool bar.

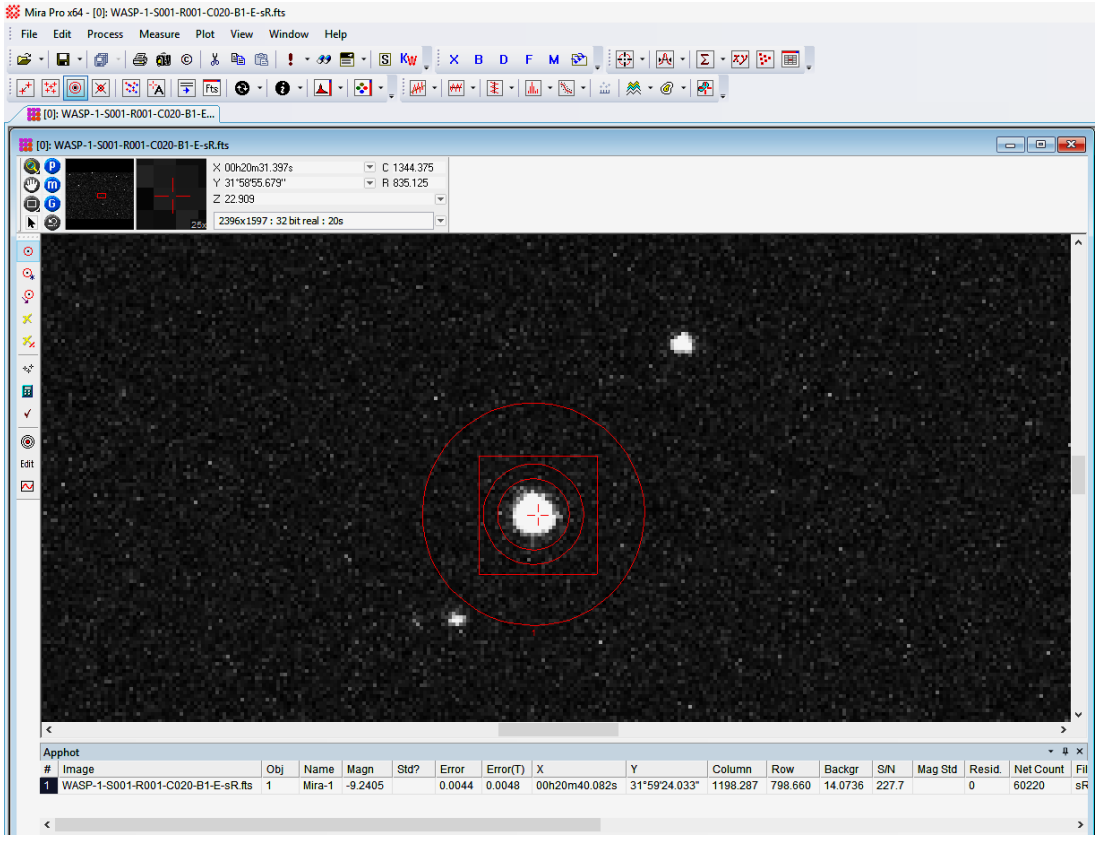

Figure 3-12: Photometry Menu In Mira

Then locate the target star and click the center to place apertures just like in Maxim DL (Fig. 3-12). The radii of the aperture, gap width, and annulus will need to be adjusted (Fig. 3-13) just like in Maxim and for the same reasons as previously discussed. The same is true for the apertures of the reference stars being used.

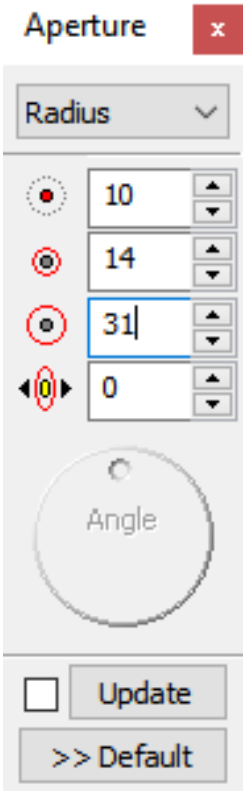

Figure 3-13: Adjust Aperture Radii

Once the sizes have been chosen, update and set as default, so Mira will remember the sizes for later.

To perform photometry in Mira Pro x64, it is necessary to create a text file with specific parameters that Mira can read, in this case referred to as a comps file. It requires a column designating the name/label for each star, the right ascension, the declination, the type designation, and magnitude in whichever filter was used for the images. The type designation refers to whether the star is the target, a reference star, or a check star (which is used to check the consistency of the reference stars). Reference stars are denoted with an asterisk, while check stars and the target are denoted with one space. Once the comps file is created, open the aperture photometry properties menu (Fig. 3-14).

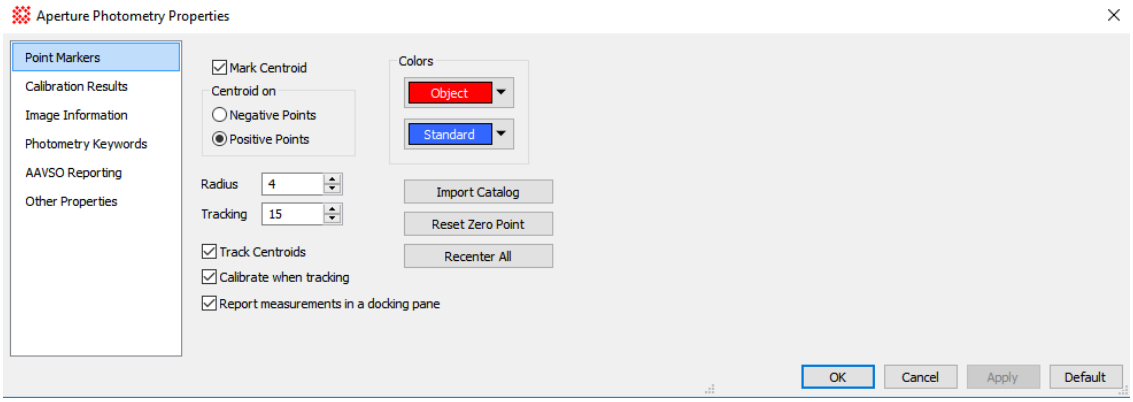

Figure 3-14: Aperture Photometry Properties

Select the import catalog to go to the import photometry catalog (Fig. 3-15).

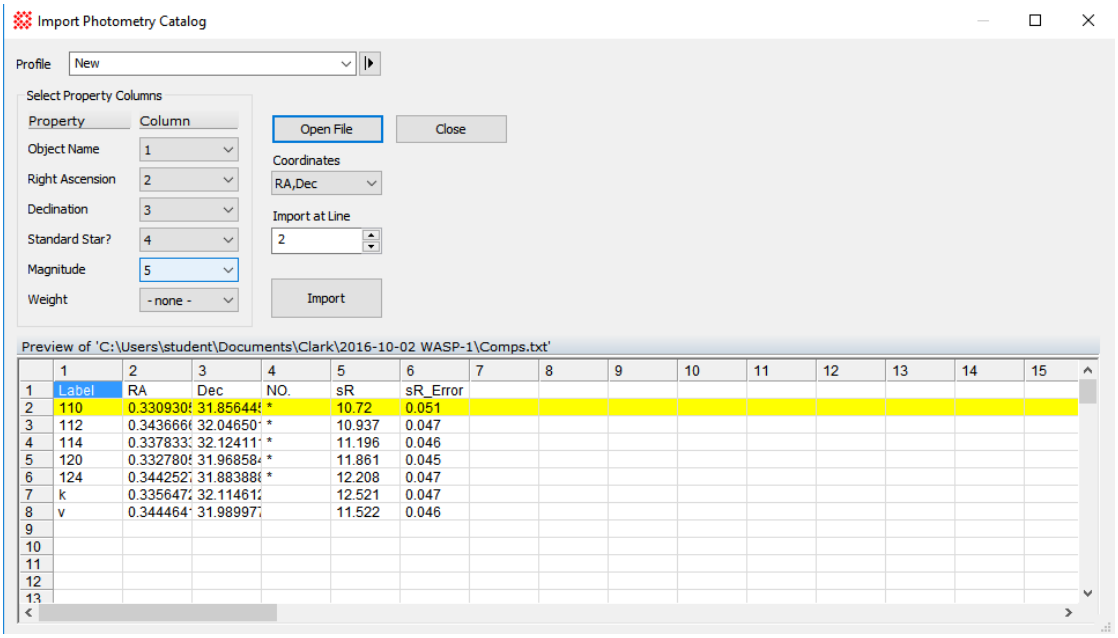

Figure 3-15: Import Photometry Catalog

Press open file to open the comps file, which will be shown at the bottom of the menu. Designate which values are in which column via the properties dropdown menus, and set it to import starting at line 2, so that it does not attempt to read the column headings. Then hit the Import button. Mira will read the comps file, and use the right ascension and declination coordinates of each star to locate them and place apertures around them, label them, and use the given magnitudes to perform all the necessary photometry measurements (Fig. 3-16).

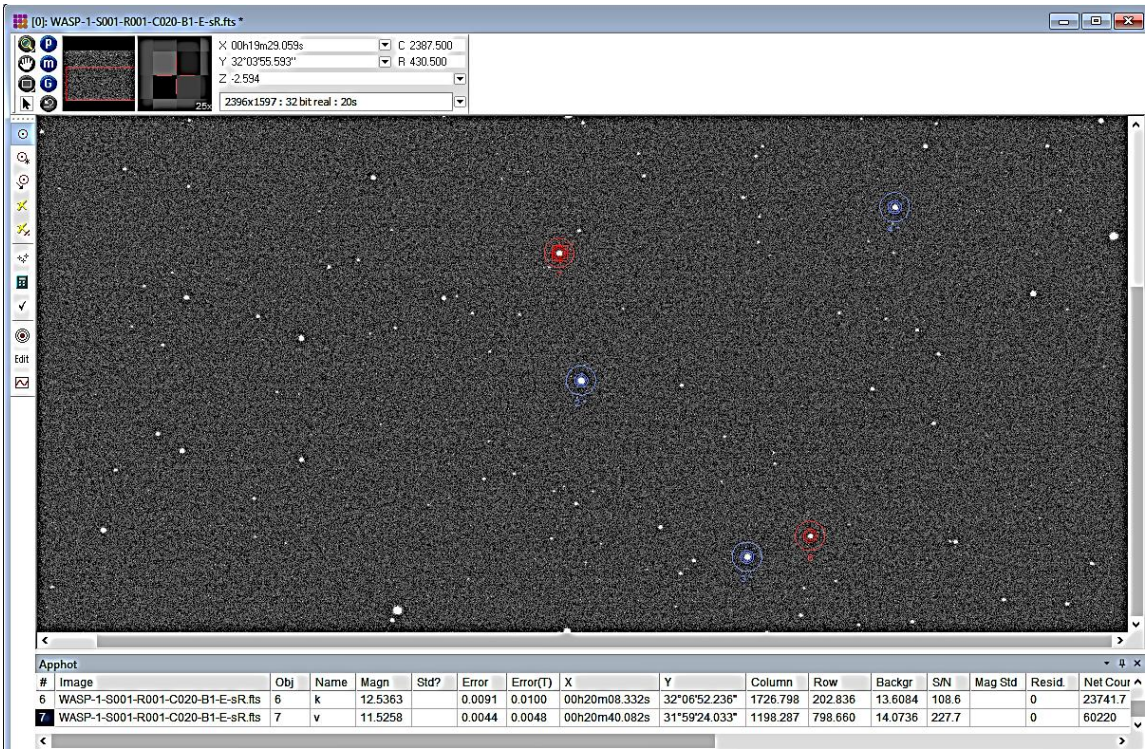

Figure 3-16: Photometry Results From Mira

Once Mira finishes analyzing the target and reference stars, the results are listed at the bottom of the screen under Apphot. Right click the bar and save all the data as an excel file. Once opened, the data will need to be rearranged and sorted to be more easily readable and to graph the magnitude and time of just the target star to generate the light curve exhibiting the transit dip.

Results

The following (Fig. 3-17) is the first magnitude versus time plot obtained.

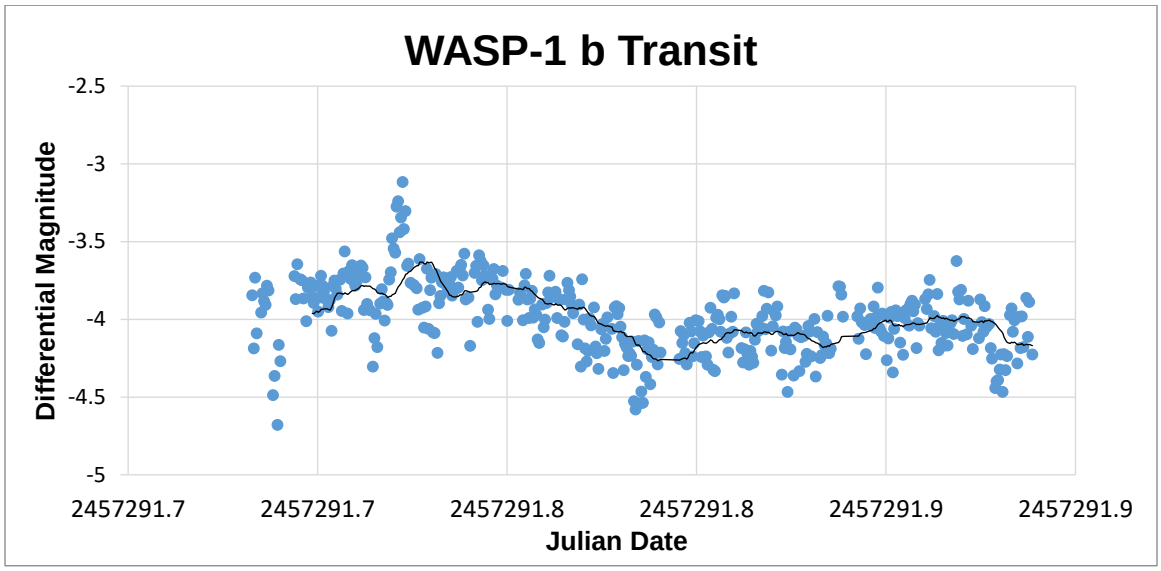

Figure 3-17: WASP-1 1st Light Curve

One problem encountered was the lack of flat fields at the time of the observations, which prevented any flat field corrections during analysis, since the flat-fields acquired later were made under different conditions and added noise to the images rather than reducing it. There was also an interruption half way through as the telescope had gone out of focus and had to be refocused manually.

The following light curve (Fig. 3-18) is from the second observing run, looking at a different target, and is incomplete.

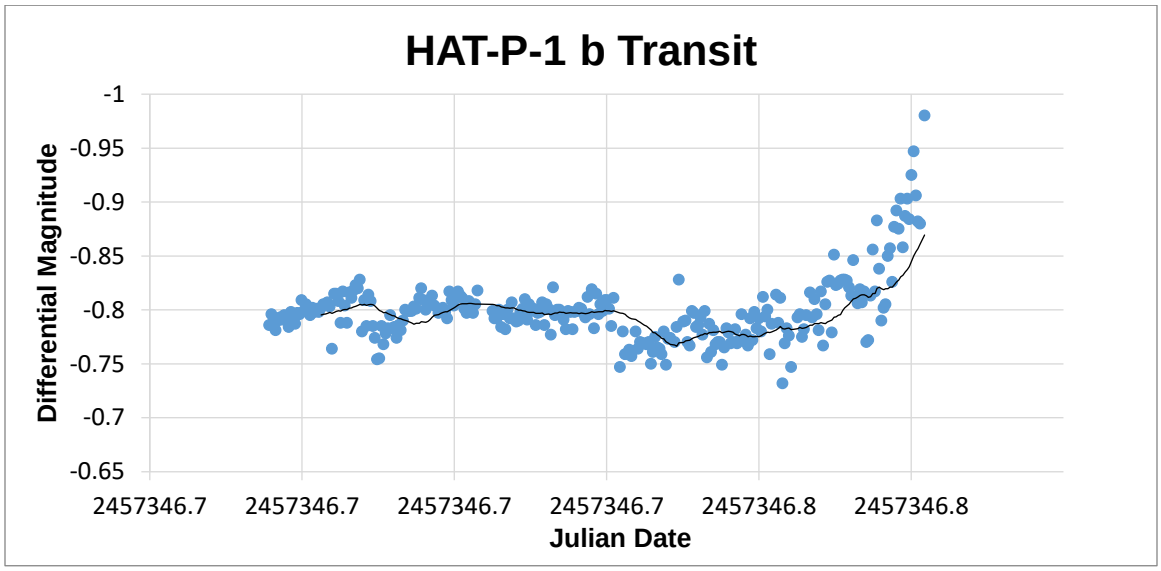

Figure 3-18: HAT-P-1 1st Light Curve

This observation yielded few results due to several issues. The telescope was poorly aligned and subsequently caused difficulties in locating the target star. The CCD camera had an auto-dark subtraction setting activated that was not discovered until after imaging had begun. This feature caused discrepancies in the images, which led to the exposure time to be set for 15 seconds which is far longer than is ideal. Once discovered and deactivated, the corrected 3 second exposure images were begun, but not until an hour after the transit had begun. Two hours before the transit was to end, the target star dipped below the edge of the roll-off roof of the telescope housing, preventing further imaging.

The first curve obtained in the spring is shown below (Fig. 3-19).

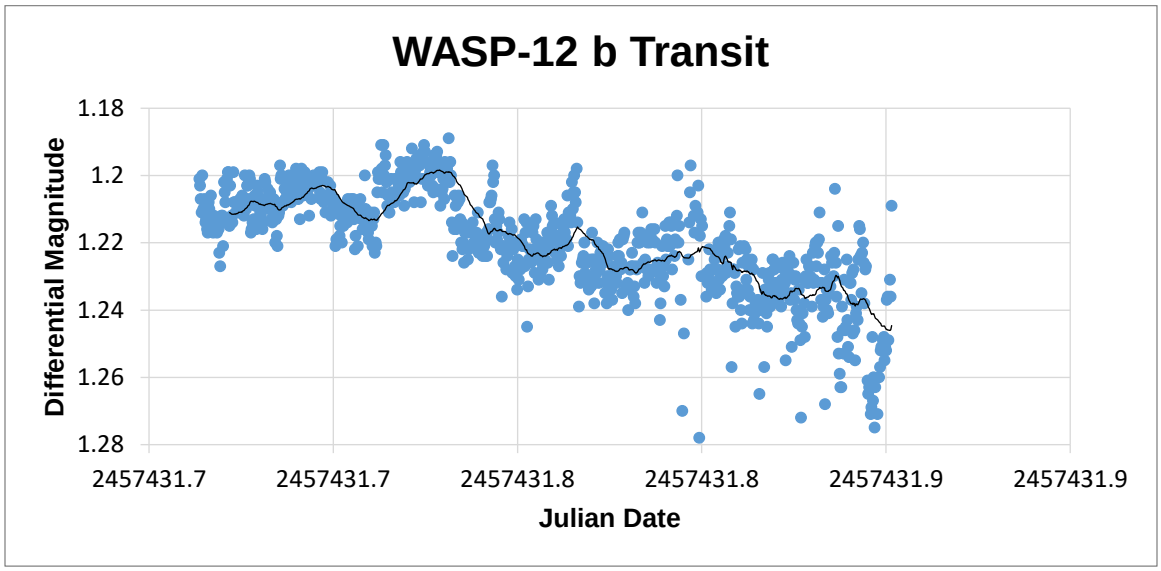

Figure 3-19: WASP-12 Light Curve

As with Hat-P-1b, the target star dipped below the roof near the end of the observing run. The data collected does not show an apparent light curve expected of an exoplanet transit. One possible explanation for this is the poor tracking of the telescope, requiring the target star to be manually re-centered in the field of view periodically.

The following (Fig. 3-20) is the second observing run of the spring semester.

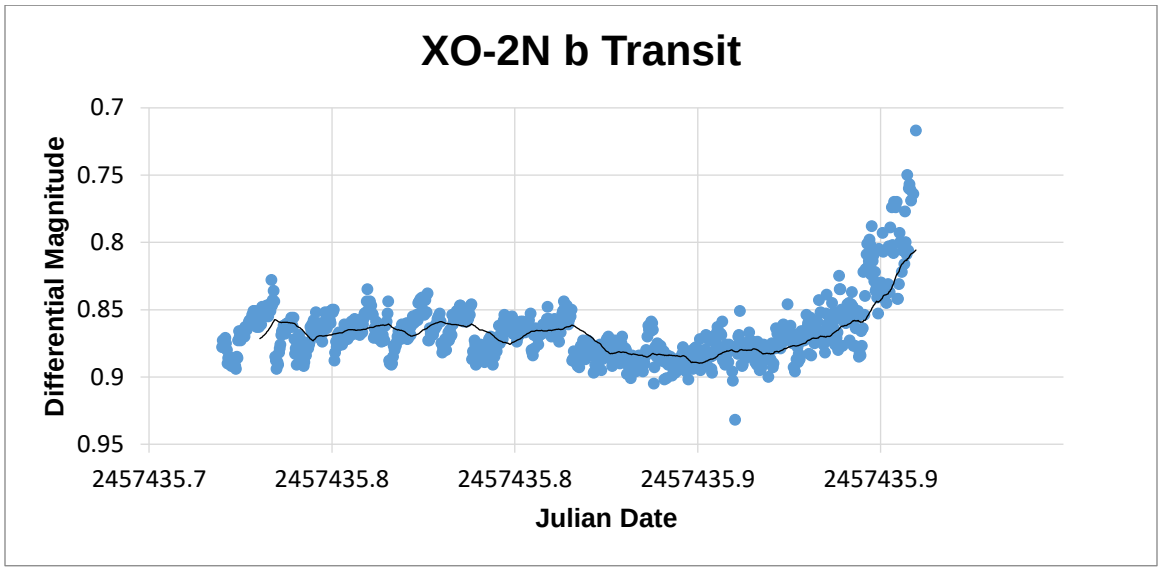

Figure 3-20: XO-2N Light Curve

Once again the target star was blocked by the roof at the end, a problem caused by the small number of possible targets that are within the viewing window while still meeting the chosen criteria. Except for the loss of the target at the end, however, this observation run went well, with good clear data obtained and a clear dip in the curve indicating the presence of a planet.

The final observation of the spring was of Hat-P-3b (Fig. 3-21).

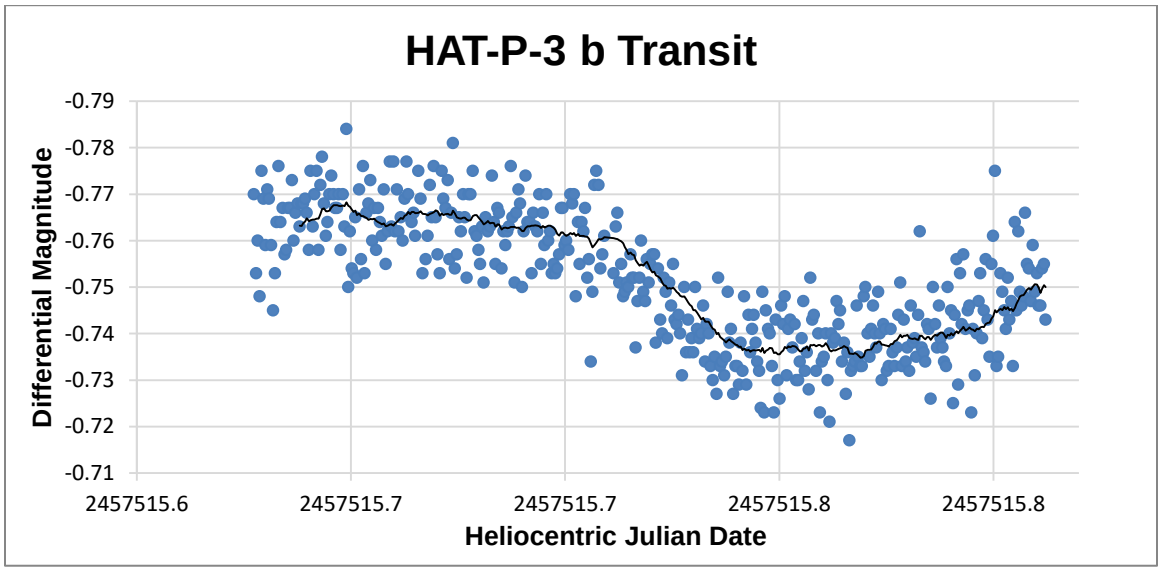

Figure 3-21: HAT-P-3 Light Curve

One problem with this observation was the slow buildup of condensation on the primary lense of the telescope. As a result, the observation had to be temporarily halted while the condensation was cleared away manually with a hairdryer. This resulted in poor images that were unable to be processed. Instead, images of the same target on the same night were aquired by Edward Michaels, using the Waffelow Creek observatory, and given to me to be processed using the same procedures as the previous data reductions to produce the light curve shown. These images were 20s exosures with 1x1 binning and used a Sloan Red filter. In addition to the dark frames and flat frames, bias frames were aquired as well.

This created an excellent light curve with a clear dip representing a planet passing in front of the star. The predicted ingress and egress of the transit were off causing the transit to appear on the second half of the light curve, possibly cutting off the true egress of the transit.

The first target observed during the following fall semester was HAT-P-1 on October 1, 2016 (Fig. 3-22).

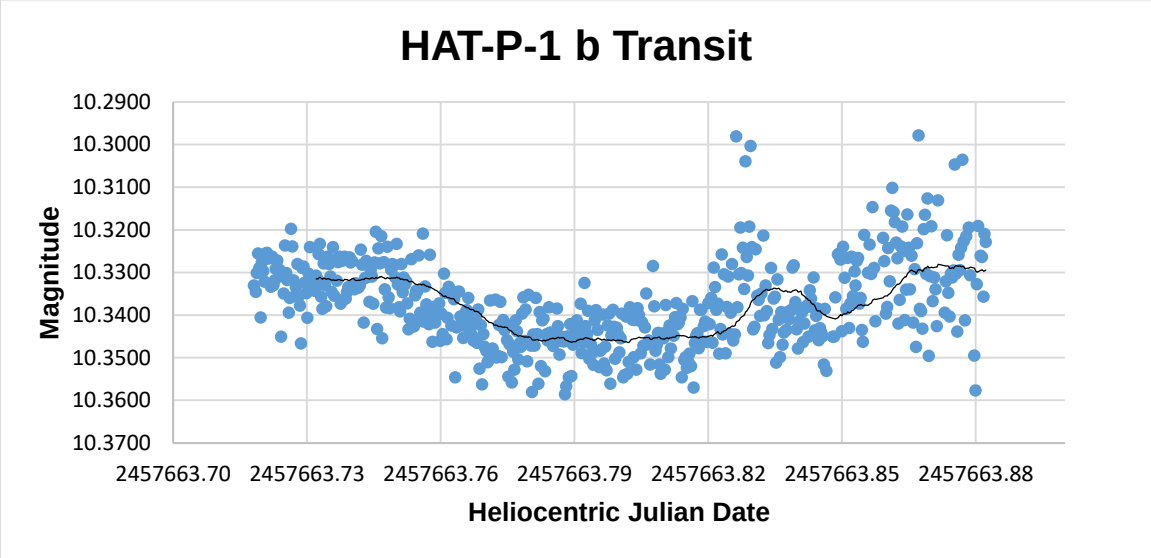

Figure 3-22: HAT-P-1 2nd Light Curve

The seeing conditions on this night were excellent until roughly 3 hours after the beginning of the observation when some cirrus clouds moved in. This can be seen in the light curve as there is an area where the magnitude suddenly spikes due to the brightness of these clouds reflecting ambient light. In addition, the data points near the end of the curve become increasingly scattered. Despite

this, the observation was able to continue and obtain usable images until 30 minutes before the scheduled end time when the clouds finally obscured the target star completely. Even with the decreased quality of the images in the latter half, the characteristic dip indicating an exoplanet transit is still clearly visible.

The next observation target was WASP-1 on October 2, 2016 (Fig. 3-23).

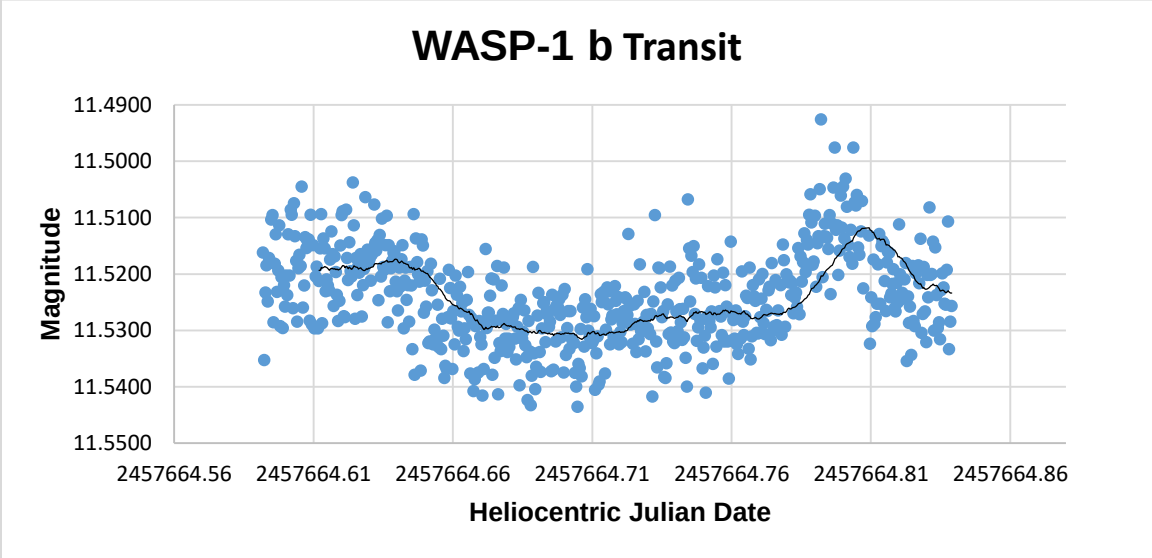

Figure 3-23: WASP-1 2nd Light Curve

This observation went as smoothly as planned with clear skies, excellent seeing conditions, and no unexpected issues. The timing of the star crossing the meridian allowed the meridian flip to be performed after the exoplanet's egress, eliminating any extended breaks in the imaging process.

The final observation of HAT-P-1 occurred on October 10, 2016 (Fig. 3-24).

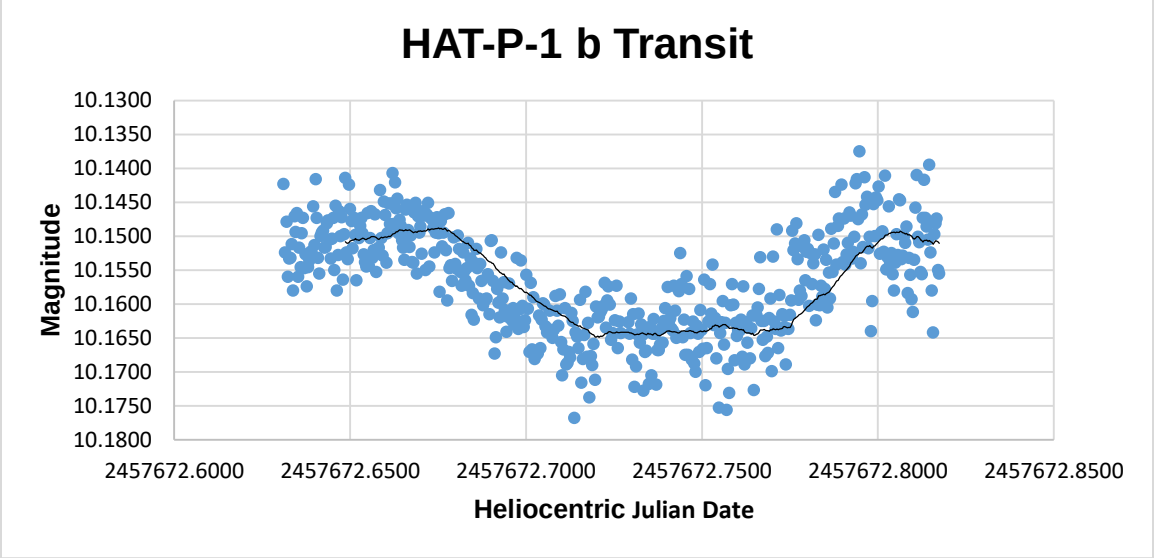

Figure 3-24: HAT-P-1 3rd Light Curve

The sky conditions remained clear for the majority of the observation, with some low clouds rolling in near the end. These clouds however, were thin, and did not cause significant variation in the data. The seeing on this night was good throughout the observation, though the image resolution was not high enough to fully separate the target and its companion. The presence of a bright moon throughout the observation was mitigated by the use of the sR filter reducing the amount of light from the moon detected by the imager. A meridian flip also had to be taken into account. Due to the position of the target, the flip could not be timed to occur before or after the transit occurred, as was the case for the two

previous observations. In this instance, it occurred at the half way point of the transit. After the meridian flip, the telescope centered on the target star's companion instead of the target, affecting the differential magnitudes during processing. This was accounted for by creating an offset correction value by averaging the data points from the first half and comparing it to the average of the second half data points, thereby correcting the issue. The result is a cleaner and more usable light curve for HAT-P-1.

Light Curve Modeling

In order to upload data to PHOEBE, it must first be converted into a format that the software can read. The input files should contain three columns with column one being phase, column two is the differential magnitudes, and the third column is weight. The phase can be acquired from the Heliocentric Julian Dates of each of the images. It is calculated from the equation

$$\text{Phase} = \frac{(\text{HJD} - \text{HJD}_\text{O})}{\text{T}}$$

Where HJD is the heliocentric Julian date of each image, HJD_O is the heliocentric Julian date of the midpoint of the transit, and T is the orbital period. The magnitudes are already in the correct format, and the weight is 1 for all the images, as that is what was used during processing. The magnitudes and weight do not need to be altered. The three columns are then put into the Notepad++

software, which is not only a text editor, but a source code editor, allowing the columns to be read as code readable by PHOEBE.

Upon start up, PHOEBE will default to the “Data” tab screen as shown below in figure 3-25.

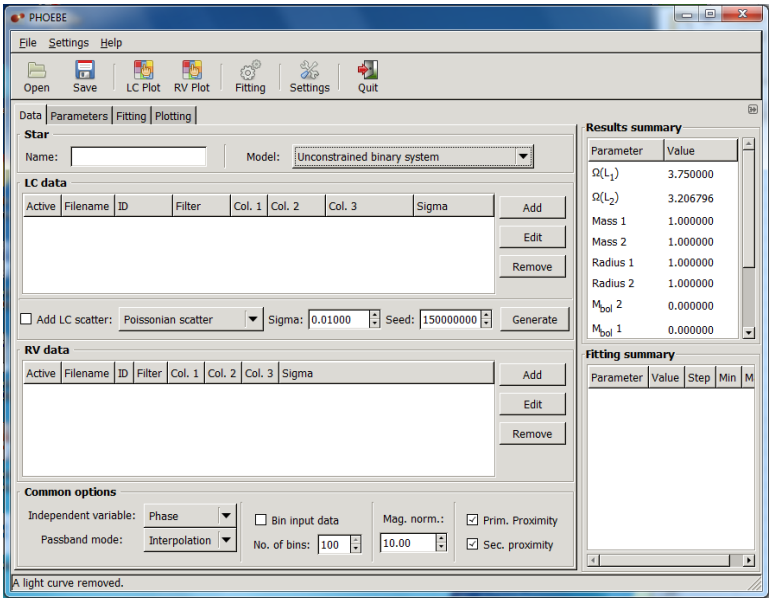

Figure 3-25: PHOEBE Start Up Screen

Change the model type from the default (Unconstrained binary system) to Detached binary. To load the data, go to LC (Light Curve) data and select Add. This will bring up the Add LC Data Menu as shown below in figure 3-26.

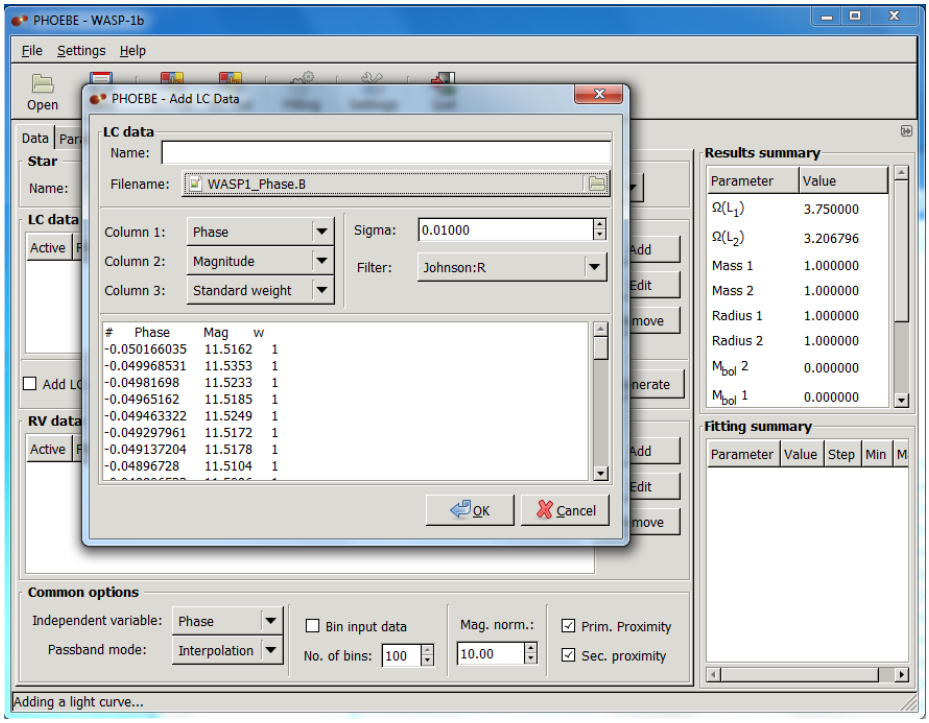

Figure 3-26: Add LC Data Menu

Select the file to be loaded, then change column 1 to Phase and select the filter used. For the stars being modeled here, an sR filter was used but is not an available option within this version of PHOEBE, so Johnson:R standard filter was used as the closest approximation.

The parameters that will be experimentally determined from modeling are the mass of the planet, the radius of the planet, the semi-major axis, and the orbital inclination. Using solely the light curve, without radial velocity measurements, it is not possible to determine all system parameters. Therefore these parameters will be approximated by using the ratios between the star and

planet. The orbital periods, host star radius, host star temperature, host star metallicity, and host star mass (for the purposes of calculating necessary ratios) were obtained from the Extrasolar Planets Encyclopaedia (Exoplanet TEAM 2015) and used as input parameters (Table 3-1). Additionally, the Heliocentric Julian Date of the center of the observed transit was obtained from the Exoplanet Archive (Exoplanet Archive n.d.). Other input parameters were determined by restrictions of the software. The planet temperatures were set at 3000K (comparatively low, however this parameter is not relevant to the fit). The primary and secondary albedo coefficients are assumed to be 0.5 while the gravity brightening coefficients are assumed to be 0.32, both due to none of the temperatures of the parent stars exceeding 7200K (Poddany 2008). The albedo of a star is how much radiation it reflects while gravitational brightening occurs when a star has larger a larger radius at the equator due to rotation, cause temperture variations across the surface, thus causing variations in brightness. Each of these are located under the “Parameters” tab and its associated subgroups. Additionally, due to the small mass ratios and low luminosities of exoplanets, some of the default values in the PHOEBE code had to be changed. The default iteration step for the primary and secondary surface potentials was changed from 0.1 to 0.01 in order to properly model the data when the mass ratio is less than 0.01 (which it will be). The “Stellar surface fine grid raster,” located under the “Fitting” tab, was increased from 20 to 60 and “Stellar surface coarse

grid raster" was increased from 5 to 15 (Poddany 2008). Lastly, the eccentricity was kept at zero, otherwise the software crashed when attempting to produce the LC plot.

Star	Orbital Period (days)	Solar Radius (R_s)	Solar Mass (M_s)	Temperature (K)	Metallicity
WASP-1	2.51995	1.382	1.24	6200	0.23
HAT-P-1	4.4653	1.174	1.151	5980	0.13
HAT-P-3	2.899703	0.799	0.917	5224	0.41

Table 3-1: Initial Input Parameters
Known characteristics of the host stars and exoplanet orbits that will be used during the modeling process.

The fitting process for each system was started with a mass ratio of 0.1, semi-major axis of 10 solar radii, and an inclination of 80 degrees. The primary and secondary surface potentials for both systems are calculated within the software (Fig. 3-27).

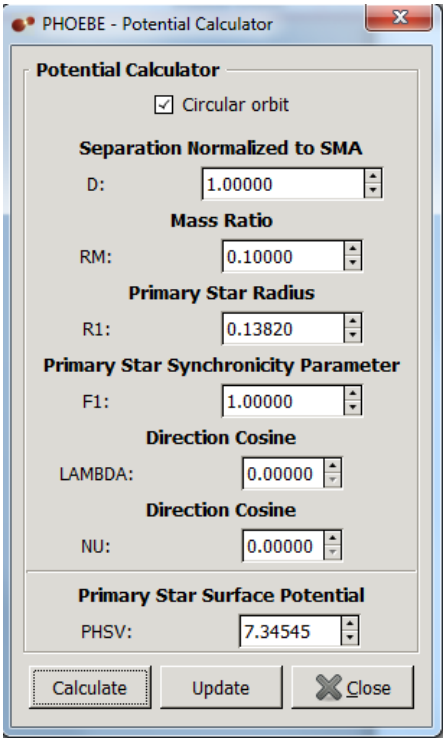

Figure 3-27: Potential Calculator Menu

The mass ratio will automatically be the same as the mass ratio input elsewhere. The star\planet radius is actually the radius divided by the semi-major axis. Leaving the other values as default, the surface potential can be calculated and then updated in the input parameters. The primary and secondary luminosities are also fitted by having PHOEBE calculate them. Limb darkening is accounted for with logarithmic limb darkening (the default in PHOEBE), with the coefficients for fitting interpolated by PHOEBE using Van Hamme limb darkening tables.

In order to fit the synthetic light curve to the data, the desired parameters are changed incrementally. The mass ratio is decreased by increments of 0.02,

and subsequently the surface potentials are recalculated, and the luminosities refitted, until the synthetic curve is approximately even with the data curve, or fitted. From here, the inclination and semi-major axis parameters are also changed in combination with the mass ratio and planetary radius in different combinations until the synthetic light curve is a good match to the observed light curve.

The results for the semi-major axis and inclination can be read directly under the “System” tab. The masses and radii of the system components are shown directly in the results summary table.

Results of Modeling

Only three light curves (HAT-P-3b, the second for WASP-1b, and the third for HAT-P-1b) were modeled. These three were chosen because they were the only three observations that produced clear, smooth light curves; the smoothest light curves with the fewest anomalies were chosen for the targets that produced more than one usable light curve. Below are the fitted curves from PHOEBE of the three light curves followed by a table of the modeled values compared with the values obtained by other astronomers.

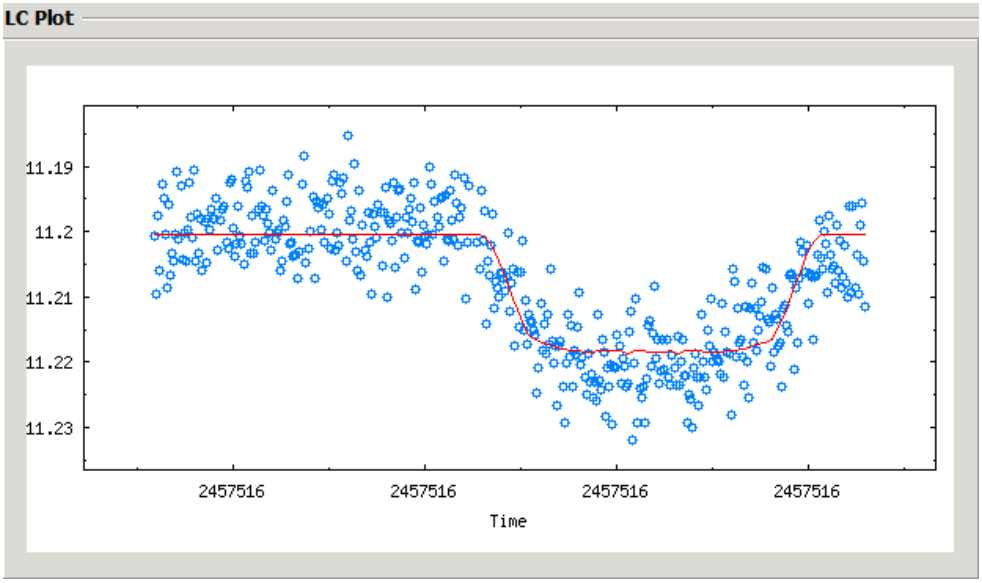

Figure 3-28: HAT-P-3 Fitted Curve

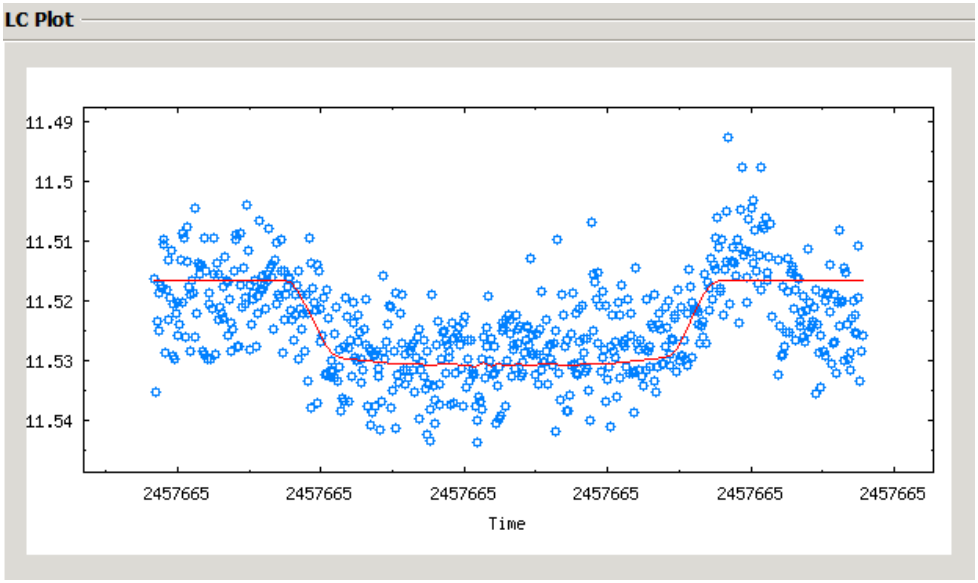

Figure 3-29: WASP-1 Fitted Curve

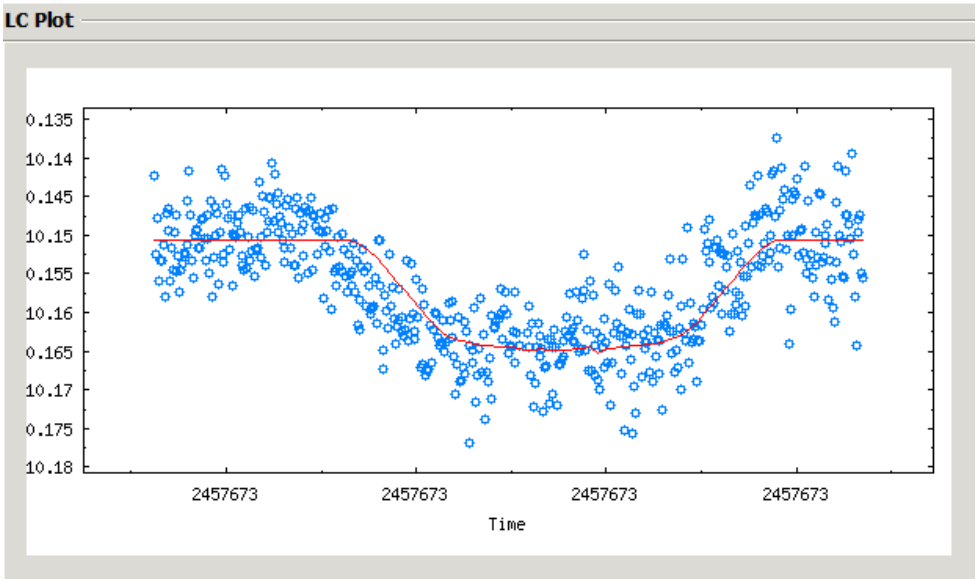

Figure 3-30: HAT-P-1 Fitted Curve

Planet	Mass (M_J)		Radius (R_J)		Semi-Major Axis (AU)		Inclination (deg.)	
	Obs.	Data	Obs.	Data	Obs.	Data	Obs.	Data
WASP-1 b	0.812	0.860	1.485	1.484	0.03813	0.03820	88.650	88.650
HAT-P-1 b	0.531	0.525	1.321	1.319	0.05557	0.05560	85.500	85.634
HAT-P-3 b	0.597	0.591	1.001	0.827	0.03953	0.03866	87.100	87.070

Table 3-2: Results Compared to Other Data
The results obtained from modeling with PHOEBE (Obs.) compared with the data from other astronomers (Data). (Exoplanet TEAM 2015)

Planet	Mass	Radius	Semi-Major Axis	Inclination
WASP-1 b	5.742	0.067	0.18341	0.000
HAT-P-1 b	1.136	0.152	0.05397	0.157
HAT-P-3 b	1.010	19.037	2.22535	0.034

Table 3-3: Percent Difference
Percent difference between the research results and the results obtained from other astronomers.

Conclusion

Multiple star systems were observed that possessed known transiting exoplanets. The data acquired from the observations were used to successfully create photometric light curves revealing the presence of the planet. Using the PHOEBE 0.31a code, the light curves were modeled to successfully determine the masses, radii, semi-major axes, and orbital inclinations of the exoplanets. When compared to the values obtained by other astronomers, the results are in good agreement.

The drop in magnitude caused by an exoplanet transit is small making the observations susceptible to several sources of errors. The primary issue encountered during observations at the SFA observatory was telescope tracking. The 16” telescope was not able to keep the target in the center of the image requiring it to be re-centered throughout the observations. As the target moved across the field of view, the image was formed from different pixels in the CCD

imager. This created small inconsistencies between each image because of small variations in the sensitivity of each individual pixel. As a result, the changes in the measured brightness of the target from image to image was not properly accounted for and effectively obscured the miniscule dip in the overall magnitude. There are several solutions to correct this issue, including adjusting the mount, adjusting gears within the telescope, and installing tracking and automation software such as ACP. Work began on the 16” to apply these fixes, however, it could not be used for detailed observations during this process. Instead, the observations were moved to the Waffelow Creek Observatory, which can track with excellent precision.

Due to the small changes in magnitude involved, it is also important to account for any background noise in the images. The best results were obtained with the use of flat frame, dark frame, and bias frame corrections to remove as much of the background noise as possible. Depending on the seeing conditions and the phase of the moon, switching from a clear or visible filter to a red filter will increase the quality of the data. There can be excess blue light from the atmosphere and other light pollution as well as light from other bright sources such as the moon or nearby bright stars. A red filter can significantly reduce the excess light in order to better see the light from the target. Binning the data can also affect the quality of the images. Changing the binning to account for differences in the quality of the seeing during each observation will also improve

the data. Generally, the best results are obtained when the binning is chosen such that the Full Width at Half Maximum is between 2 and 3 pixels. Lastly, it is beneficial to take to Signal to Noise Ratio into account as it indicates the quality of the seeing on a given night with higher SNR indicating good conditions. The filter and binning should be chosen to maximize the SNR in order to obtain high quality results.

The results obtained from modeling the light curves with PHOEBE were successful. The percent differences between the research results and the comparison data were small for the most part. The only exceptions were the mass of WASP-1b (5.742%) and the radius and semi-major axis of HAT-P-3b (19.037% and 2.225% respectively). The main issue arises from the few available observations. The models for each star were produced from a single observation of each, whereas the comparison values are averages of many observations from several locations. This means that any errors resulting from weather and equipment malfunctions have a greater effect without other observations to counteract the effects. HAT-P-3b in particular had the largest percent differences overall compared to the other two models. This was most likely due to the poor seeing conditions and weather on that night. However, it is possible that the percent difference was due to HAT-P-3b being smaller than the other two which could cause modeling difficulties since PHOEBE is originally

designed to model binary stars. This could explain why the mass parameter had overall higher percent differences compared to the other output parameters.

Even with these errors, however, the results were still similar to the compared values indicating the effectiveness of the data collection as well as the modeling predictions. Although the process of observing a transiting target to obtain data is time consuming, it is effective in finding and confirming the presence of an exoplanet about a star. Additionally, PHOEBE is a quick and effective tool for determining physical and orbital characteristics of transiting exoplanets.

BIBLIOGRAPHY

Ed. Arielle Samuelson. n.d. NASA. <https://exoplanets.nasa.gov/interactable/11/>.

n.d. <http://www.planetary.org/explore/space-topics/exoplanets/how-to-search-for-exoplanets.html>.

2012. <https://ria.ru/science/20120206/558647431.html>.

n.d. <http://var2.astro.cz/ETD/>.

n.d. NASA Exoplanet Science Institute. <http://exoplanetarchive.ipac.caltech.edu/>.

n.d. <https://www.eso.org/public/archives/presskits/pdf/presskit_0005.pdf>.

n.d. <https://www.aavso.org/>.

ACP Observatory Control Software. n.d. <http://acp.dc3.com/index2.html>.

"Alnitak Flat-Man XL Flat Fielder." n.d. Optec optical and electronic products. <http://www.optecinc.com/astronomy/catalog/alnitak/flatmanxl.htm>.

Burke, Christopher J, et al. "XO-2b: Transiting Hot Jupiter in a Metal-Rich Common Proper Motion Binary." *The Astrophysical Journal* (2007): 2115-2128.

Chan, Tucker, et al. "The Transit Light-Curve Project. XIV. Confirmation of Anomalous Radii for the Exoplanets TrES-4b, HAT-P-3b, and WASP-12b." *The Astronomical Journal* 141.6 (2011).

Collier Cameron, A, et al. "WASP-1b and WASP-2b: Two new transiting exoplanets detected with SuperWASP and SOPHIE." *Monthly Notices of the Royal Astronomical Society* 375.3 (2006): 951-957.

Exoplanet TEAM. 2015. <http://exoplanets.eu/>.

Hebb, Leslie, et al. "WASP-12b: The Hottest Transiting Extrasolar Planet Yet Discovered." *The Astrophysical Journal* 693 (2009): 1920-1928.

Laughlin, Gregory. 2009.

Many Astronomers. *PHOEBE Project*. n.d. <http://phoebe-project.org/>.

Maxim DL 5. 1996. Diffraction Limited. <http://www.cyanogen.com/index.php>.

Mayor, Michel and Didier Queloz. "A Jupiter-mass companion to a solar-type star." *Nature* 378.6555 (1995): 355-359.

Michaels, Edward J. n.d. <http://obs.ejmj.net/>.

Poddany, Stanislav. "How to use the Phoebe code to solve transiting exoplanet light curve." *International Astronomical Union*. Prague, 2008.

Starling, David. 2014. <http://www.personal.psu.edu/djs75/research.htm>.

The Sky X. 2015. Software Bisque. <http://www.bisque.com/sc/pages/TheSkyX-Professional-Edition.aspx>.

Torres, G, et al. "HAT-P-3b: A Heavy-Element-Rich Planet Transiting a K Dwarf Star." *The Astrophysical Journal* 666 (2007): L121-L124.
Waldmann, Ingo. *L11: Finding exoplanets the Transit technique*. n.d. <http://zuserver2.star.ucl.ac.uk/~ingo/Lecture_Notes_files/lect11.pdf>.
Wilson, Paul Anthony. "The exoplanet transit method." 2016. *Paulanthonywilson.* <https://www.paulanthonywilson.com/exoplanets/exoplanet-detection-techniques/the-exoplanet-transit-method/>.
—. "The Transit Light Curve." 25 January 2013. *AAVSO.* <https://www.aavso.org/files/exoplanet-transits-wilson.pdf>.

VITA

Clark Holcomb graduated from The Colony High School in June of 2010 and promptly enrolled at Stephen F. Austin State University. In May of 2014 he received a Bachelor of Science in Physics from SFA before enrolling in Graduate School in the Department of Physics and Astronomy. Throughout this time he has worked as an undergraduate teaching assistant, then as a graduate teaching assistant, as well as a Planetarium presenter, all within the same department. He is currently working toward completing his Masters of Science.

Permanent Address: 4309 Biscayne Drive
The Colony, TX 75056

Style MLA form

This Thesis was typed by Clark Holcomb.